Available online at www.sciencedirect.com
SCIENCE DIRECT®
Journal of Nuclear Materials 336 (2005) 331–368
journal of nuclear materials
www.elsevier.com/locate/jnucmat

Some thoughts on the mechanisms of in-reactor corrosion of zirconium alloys

B. Cox

Centre for Nuclear Engineering, University of Toronto, Toronto, Ontario, Canada M5S 3E4

Received 10 April 2003; accepted 15 September 2004

Abstract

In recent years sufficient new information has accumulated to change current views of which mechanisms of corrosion are operating in water-cooled reactors. The total number of publications is now so enormous that it is impossible for a short review to be completely comprehensive. This review concentrates on those studies that have resulted in changed views of the importance of various mechanisms. There seems to be insufficient evidence to support an hypothesis that increased corrosion rates in reactor result directly from displacement damage to the oxide by fast neutron bombardment. Replacing this hypothesis are the observations that redistribution of Fe from second phase particles (SPPs) into the Zr matrix by fast neutron recoil reduces the corrosion resistance of Zircaloy type alloys both in-reactor and in laboratory tests. There is little support for the idea that an irradiation induced phase change from monoclinic to tetragonal (or cubic) zirconia is important in-reactor, since such transformed zirconias are unstable in ~300 °C water and revert to the monoclinic phase; as do chemically stabilised zirconias. New alloys with improved corrosion resistance in PWRs are generally low in Fe (and Sn), or have Fe in the form of more radiation resistant SPPs than those in the Zircaloys. Similarly, the hypothesis that nodular corrosion in BWRs was directly related to an effect of irradiation produced radical species in the water is unsupported. However, local dissolution of the oxide film by radiation produced species such as H_2O_2 may be occurring, and the close mechanistic relationship between nodular corrosion and 'shadow corrosion' is very evident. Thus, galvanic potentials between large SPPs (or clusters of SPPs) and the Zr matrix, aided by greatly increased electronic conduction of zirconia in irradiated systems appears to offer an hypothesis that provides a rationale for the observed effects of SPP sizes and numbers. Irradiation induced redistribution of Fe from the SPPs into the Zr matrix eliminates nodular corrosion susceptibility in Zircaloys.

Contents

E-mail address: irenem@magma.ca

0022-3115/$ - see front matter © 2004 Published by Elsevier B.V.
doi:10.1016/j.jnucmat.2004.09.029

1. Introduction

Zirconium alloys were developed for use as nuclear fuel cladding (amongst other nuclear reactor components) in the early 1950s [1,2]. A number of reviews of their corrosion mechanisms, both out- and in-reactor, have been published since then [3–12]. The most comprehensive of the recent reviews [9,11] are unfortunately out of print, and so a further review at this time seems appropriate, especially as recently published research has resulted in significant changes to ideas of what is affecting corrosion in-reactor. It is not the intent here to match the comprehensiveness of IAEA-TECDOC-996 [11] which comprises 308 pages and 538 references. The aim will be to follow the development of an understanding of the corrosion mechanisms that operate in nuclear reactors, by citing the key pieces of research that have moulded this understanding. Wherever possible references that give a good listing of previous work in a specific area are used, so that readers will have access to the primary references – although the availability of such early references can no longer be guaranteed.

Before an assessment of the in-reactor corrosion mechanisms can be attempted, a summary of the early zirconium alloy development, and the mechanisms that operate out-reactor is necessary. If the oxidation mechanism out-reactor is not understood, useful interpretations of the in-reactor behaviour cannot be offered.

2. Development of zirconium alloys

Zirconium was chosen for use in the cores of water-cooled nuclear reactors because of its low thermal neutron capture cross-section, reasonable mechanical properties and adequate corrosion resistance in high temperature water [1,3]. It was initially thought that the poor corrosion resistance of some batches of unalloyed zirconium produced by the van Arkel process was a result of stray impurities. However, it was found that improving the purity did not eliminate these problems [1]. The oxidation rate of zirconium was found to vary considerably with grain orientation during the growth of thin, interference-coloured, oxide films

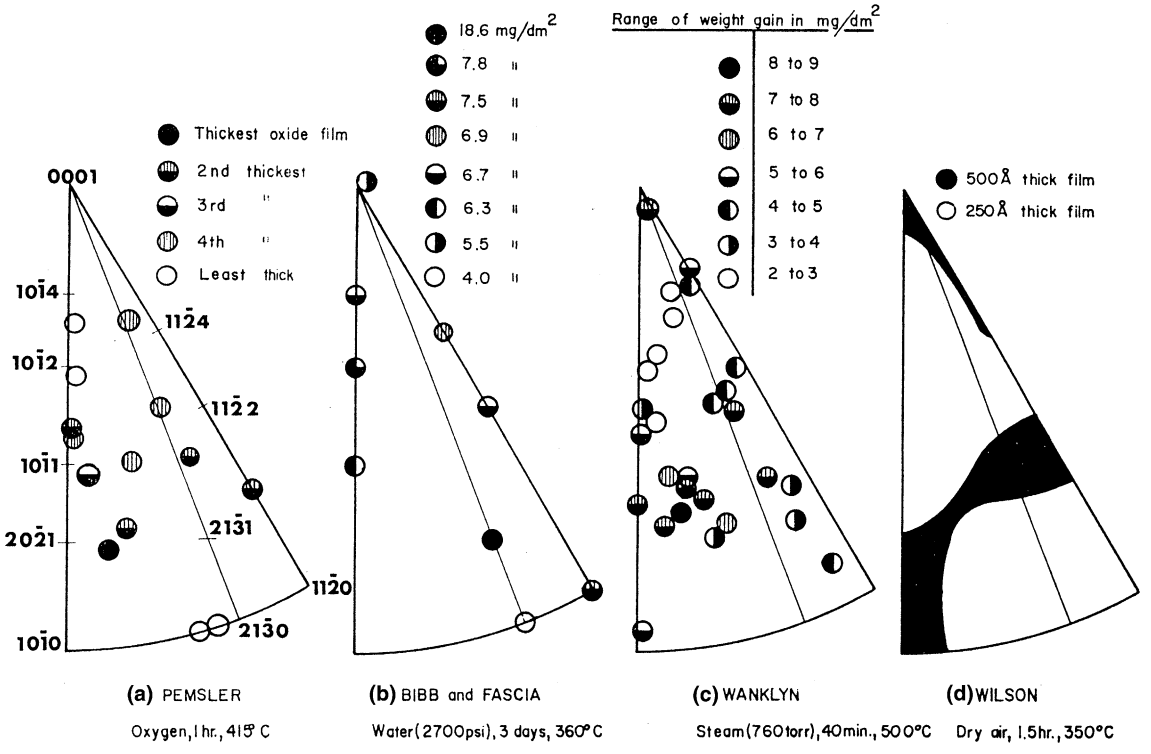

Fig. 1. Summary of available zirconium oxidation anisotropy data [13].

(Fig. 1) [13]. As these oxides thickened, and became black because of optical absorption, the differences in oxidation rates of the different grains led to severe growth stresses and cracking of the oxide at the grain boundaries separating rapidly and slowly oxidising grains [14,15]. Small regions of locally thick oxide (not unlike what would subsequently be called 'nodular corrosion') were observed predominately on grains showing the lowest oxidation rates, and ridges of similarly cracked thick oxides were formed along grain boundaries separating two slowly oxidising grains. These localised oxidation effects had apparently little effect on the oxidation rates of pure zirconium in oxygen, although they did lead to a linear growth rate [16]. In high temperature, high-pressure steam these differential oxidation rates led to oxide spalling, that was sometimes severe [14], while in high temperature water the effect could be disastrous 'breakaway' of the oxide [3].

Whether serendipitously or not, this problem was solved by the addition of transition metals (Cr, Fe, Ni), that were largely insoluble in the zirconium matrix and appeared as small particles of intermetallic phases, and tin which was soluble in zirconium and which nullified the negative effects of the nitrogen impurity [3,4,6] present in the Kroll process zirconium (cheaper than van Arkel process material). During oxidation tests in oxygen and low pressure steam the insoluble transition metals did not decrease the diffusion controlled pre-transition oxidation rates, but did result in the generally earlier onset of the linear post-transition oxidation rates (where the oxide growth has ceased to be diffusion-controlled) [16,17]. Thus, the main advantage of the alloying additions in what were now termed Zircaloy-2 and Zircaloy-4 [1] appeared to be the development of a more uniform thick oxide film that did not appear to be susceptible to early spalling. An early attempt at an explanation for this suggested that the multiplicity of small surface intermetallic second-phase particles (SPPs) accelerated the growth of the slowly oxidising grains so that the oxide became more uniform, developed less locally highly stressed regions, and so showed less cracking and spalling as it grew [18]. However, binary additions of transition metals alone, did not usually eliminate these localised corrosion effects in high temperature, high pressure (500 °C, 8–10 MPa) steam [19].

Russian developments of zirconium alloys focussed more on the effects of niobium additions, which had beneficial effects similar to tin additions, and used van Arkel process base metal containing iron contents typically higher than the solubility limit (Fig. 2) [20] so that some intermetallic particles were also present [21]. It will be seen later that two of the alloys that developed from this work (E110 – Zr–1%Nb; E635 – Zr–1%Nb – 1%Sn – 0.4%Fe) [22] were to have a profound effect on the development of new cladding alloys for Western Pressurised Water Reactors (PWRs).

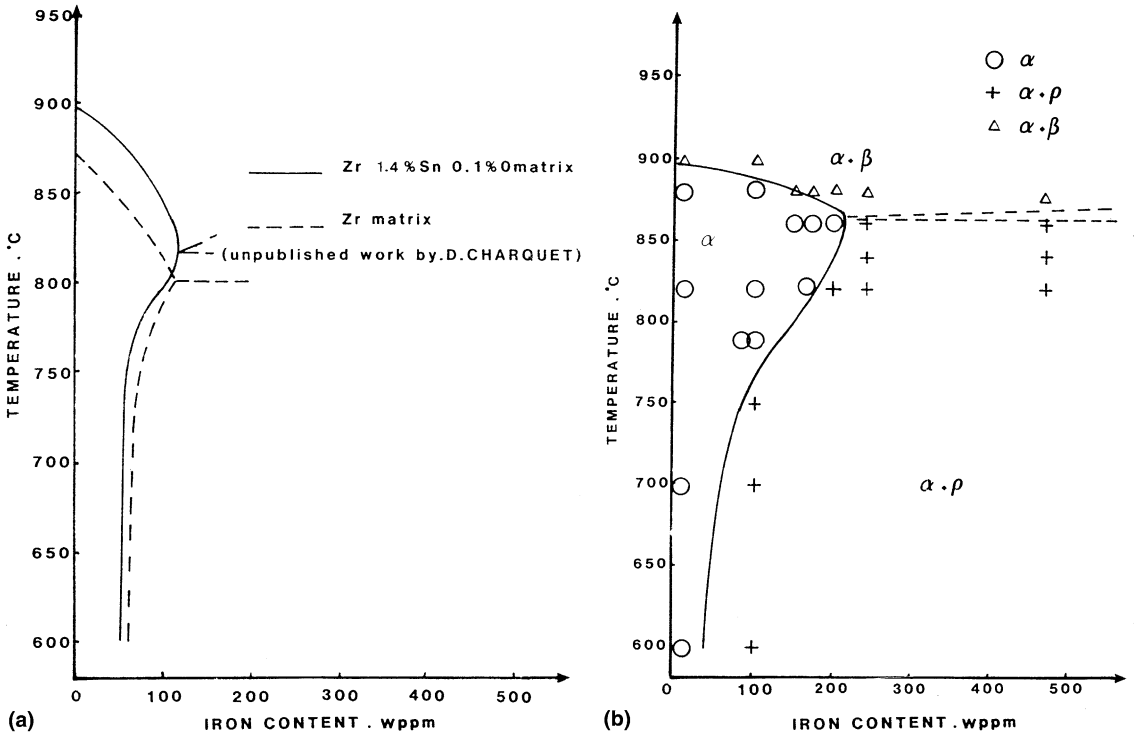

Fig. 2. (a) Comparison of the zirconium-rich corner of the systems: Zr (1.4% Sn, 0.1% O)-Fe and Zr–Fe [20]. (b) Zirconium-rich corner of the system: Zr (1.4% Sn, 0.1% O, 0.0036% Fe)-Cr [20].

3. Corrosion out of reactors

Because the pre-transition corrosion kinetics are independent of pH between about 1 and 13 (if no specifically aggressive species such as LiOH is present) and of the source of the oxygen (O_2, H_2O, O in Na/K), if other factors such as temperature and pressure are constant, it has been argued that the oxidation processes are controlled entirely by diffusion of species through the oxide film [5,6]. The recent suggestion by Bossis et al. [156] that the rates of surface reactions can be rate controlling seems to be based on the fallacious premise that this is the only way to explain the accelerated corrosion in BWR coolant, and on an inadequate metallographic technique that resulted in the production of artefacts [156]. Over the years the answers to the following mechanistic questions related to migration of charged species through the oxide film have been addressed, and in some cases partially answered:

- What are the mobile species during corrosion out-reactor, and what are their relative mobilities?
- Why does the pre-transition, diffusion-controlled kinetic period follow a rate law close to cubic, rather than the more commonly expected parabolic rate law?
- What are the processes that lead to the breakdown of this initially protective oxide film?
- What role if any does hydrogen have in the above processes?

The present status of the answers to these questions will be summarised briefly.

4. Mobile charge carriers in zirconium oxide films

In the absence of external applied potentials on the specimen there can be no net current through the oxide. Thus, the negative and positive oxidation currents must be equal and opposite. If this is not the case initially, then a potential will develop across the oxide that will equalise these currents. In ceramic zirconia specimens oxygen was established to have much higher diffusion rates than zirconium ions. Measurements using radioactive oxygen isotopes [23] showed that oxide grain boundary diffusion in thermal oxide films agreed with these measurements on stabilised, cubic ZrO_2 ceramics (Fig. 3) which have high intrinsic vacancy concentrations, while the bulk diffusion rates for oxygen were over five orders of magnitude slower and were close to estimates of diffusion in ZrO_2 with low vacancy concentrations.

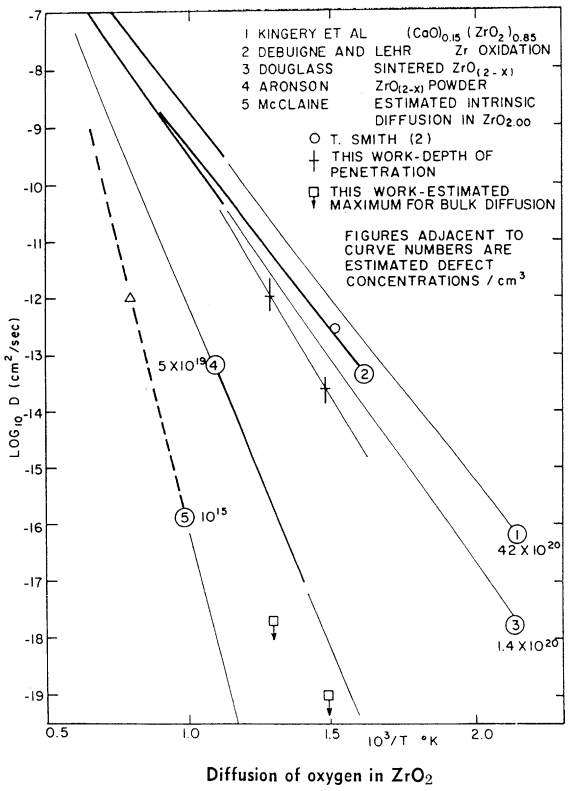

Fig. 3. Diffusion of oxygen in ZrO_2 [23].

Diffusion of zirconium ions was expected to be very low, based on its immobility during the growth of anodic oxide films [23]. However, reports of some Zr mobility at very high temperatures under LOCA conditions [24] showed that there might be some small zirconium ion migration. That this was, in fact, very small at typical power reactor temperatures has recently been confirmed [25].

Thus, if oxygen ions are the only mobile ionic species, the overall charge neutrality in the oxidation process must be achieved by the electron current flowing in the opposite direction to that of oxygen ion migration. Since zirconia is an almost completely ionic oxide there can be few free electrons, so that the electronic current is probably achieved by electron hopping from Zr to Zr. This is the equivalent of a valence change in the Zr ions, which are immobile. ZrO_2 ceramics have long been known to be good insulators [26], and recent measurements by Electrochemical Impedance Spectroscopy (EIS) have been interpreted in terms of an electrical conductivity for the stabilised zirconia grains, and a second term for the grain boundary conductivity in series with this. In stabilised zirconia ceramics the grain boundaries are the high resistance component, probably because of the presence of thin films of a glassy phase at the grain boundaries [27,28].

Measurements of the resistivities of oxide films grown on zirconium alloy specimens have also tended to be made by EIS techniques [29–32]. Although these give comparative numbers for oxides on different alloys, formed in different environments, they are of limited value mechanistically because it is not possible to derive current/voltage (I–V) curves, and hence develop information on the electronic conduction processes. I–V curves measured on specimens oxidising in high temperature aqueous electrolytes [33,34] suggest that the cathodic currents measured have been limited by the poor reversibility of the surface electrochemical processes in the aqueous electrolyte for the electron current [6]. When these I–V curves are compared with ones measured in fused salts (Fig. 4), the anodic electronic current is seen to be much less affected than the cathodic current. These same surface reactions are probably the cause of the large variability in the open circuit potentials measured in even the same nominal water chemistry [34]. However, the independence of the pre-transition corrosion rates from the water chemistry [5,6] shows that these surface reactions are not rate determining.

By analysing these I–V curves (Fig. 4) the electrical conduction in oxide films on Zircaloy-2 was determined to follow Schottky kinetics [35]. An interesting observation during these measurements involved the effect of iron oxide layers deposited on the oxide surface on the electronic conductivity [36]. It was found that a thin layer of Fe_2O_3 resulted in a large increase in the electronic conduction, whereas an Fe_3O_4 layer did not. This was interpreted as a result of 'hole injection' from the iron oxide layer because of the coupling of the respective band gaps. In the thin film region such layers may result from oxidation of surface intermetallics. For thick oxide films in reactors, however, an interaction with crud layers, depending on their chemical composition, becomes a possibility.

5. Rate determining processes

It is not easy to deduce, from separate measurements of the oxygen diffusion coefficients and the electrical conductivity of oxide films formed on zirconium alloys, which process is rate determining. However, since charge balance must be maintained between the two processes (at least on a general basis, if not on the local ionic scale as required by the Wagner/Hauffe oxidation mechanism [37]), then, if the two processes do not initially proceed at identical rates, a potential will develop across the oxide such as will slow down the faster process and accelerate the slower process to equalise the two rates. The magnitude of the resulting potential difference will be determined by the polarisability of the two diffusion processes (i.e. the slopes of their respective I–V curves) and the half-cell potentials of the anodic

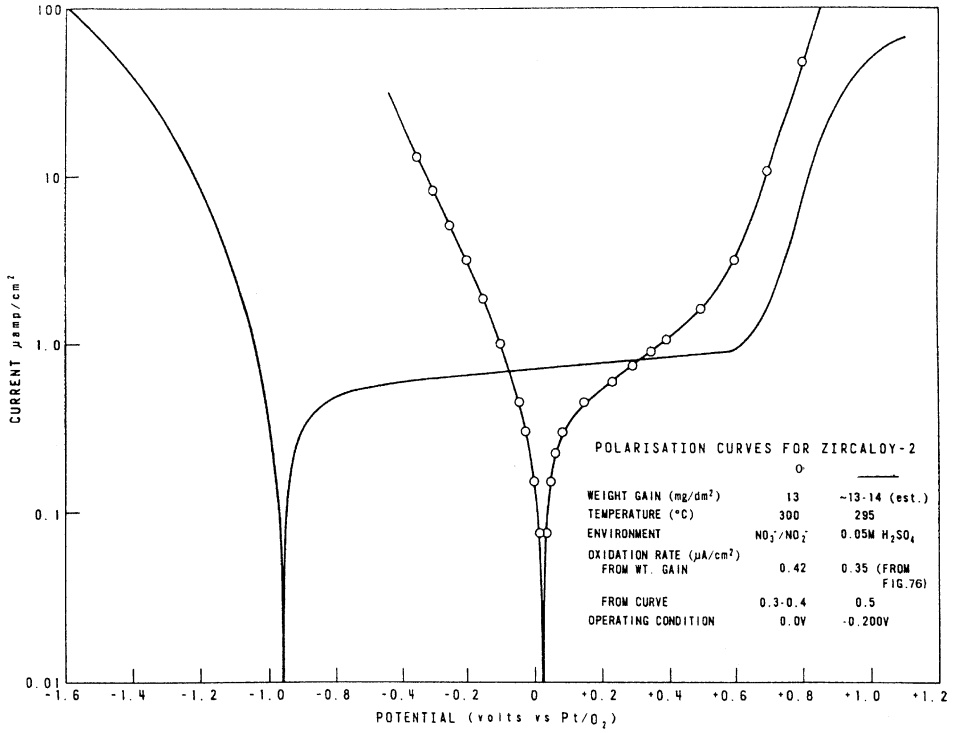

Fig. 4. Comparison of polarization curves for similar Zircaloy-2 specimens in aqueous solution and fused salt at ~300 °C [6].

(oxygen migration) and cathodic (electron migration) half-cells.

The overall potential driving the oxidation reaction has been established from the energy involved to be ~2.34V [38], but the respective half-cell potentials must be determined experimentally. Results suggest that the anodic half-cell potential (E_a) is $\sim 1.0 \pm 0.1$V, and the cathodic half-cell potential is $\sim 1.35 \pm 0.1$V. Measuring the potentials developed across the oxide film during oxidation without affecting the oxidation reaction is not easy. Experiments at high temperatures (600–800 °C) using a point probe pressed on the outer oxide surface often results in a local short-circuit, especially in the thin film region [39], as a result of oxide cracking, or lack of oxygen accessibility (or both) at the point of contact. Measurements made with evaporated metal layers, even if these are porous, also suffer from possible changes in local oxygen access [40]. Measurements in high-temperature aqueous solutions at 300 °C may be affected by the already noted lack of reversibility of the cathodic processes at the oxide/metal interface [6], and the measurements in high temperature fused salts at 300 °C may also have problems with reversibility of the cathodic process. However, at low polarisation rates cyclic tests in fused salts show little or no hysteresis [41]. This last technique has the merit that it gives results at typical reactor temperatures (apparently without the complications due to surface electrochemical reactions) and shows potentials across the oxide film that are similar to those measured by the other techniques during high temperature (600–800 °C) oxidation. It does show a drop in the negative potential at the oxide/metal interface as the oxides thicken which is not seen in the high temperature measurements, however (Figs. 5 and 6). This drop has been ascribed to the formation of an iron oxide layer on surface intermetallics, which enhances the oxide's electronic conduction [36]. Attempts to image the sites of electronic conduction by using evaporated CuI layers suggested that this process was localised at second phase particles incorporated into the oxide, at least in the thin film region [42].

Before putting much weight on these measurements of the voltage across the oxide during oxidation, the question of whether they are determined by the kinetics of migration of charged species through oxide, as described above, or are thermodynamic potentials determined by the free energies of the anodic and cathodic processes should be addressed. That they are kinetically determined is shown by the observations that, at the start of oxidation, the potential is zero and increases to the equilibrium value over a significant time; returning to zero if the oxidation is stopped (Fig. 5) [38]. Further support for a kinetic origin comes from the effect of a high temperature preoxidation, which would redistribute Fe and Cr in the oxide film, and thus change the bal-

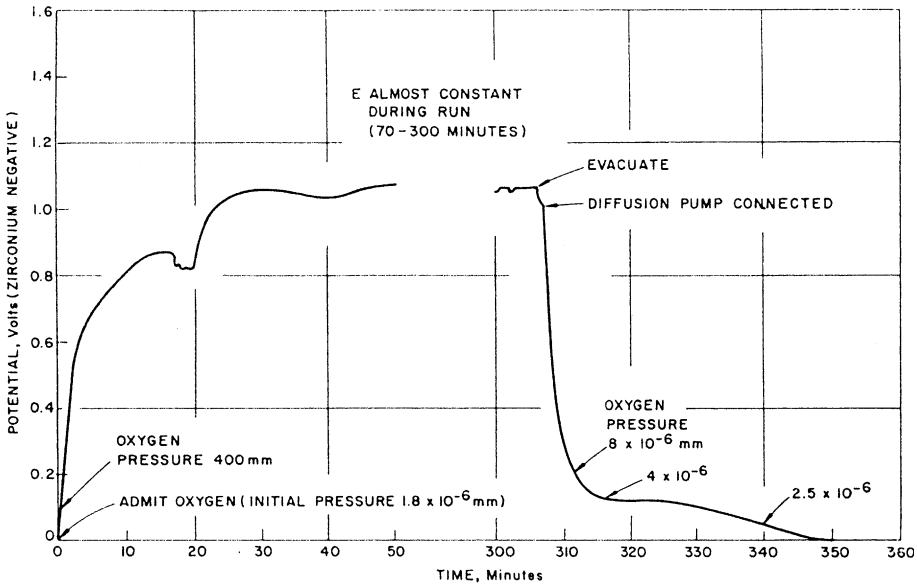

Fig. 5. Behavior of potential developed during oxidation of zirconium at 700 °C [38].

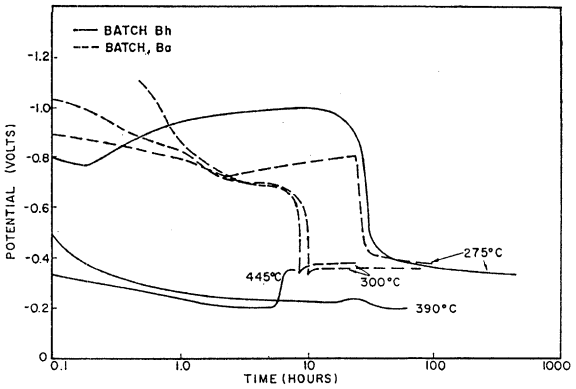

Fig. 6. Potential vs. time curves for Zircaloy-2 in fused salt [35].

ance of the migration processes, such a pre-oxidation reduces the negative potentials on the metal (and in some instances makes them positive), and at the same time results in a 'memory effect' (a short period of higher than expected oxidation) [35].

Thus, a picture emerges in which the growth of the oxide initially is controlled by the electronic conductivity of the film formed. During high temperature gaseous oxidation this control by electronic conduction continues to be evident, whereas at temperatures close to reactor temperatures it appears that the oxide may become more conducting as it thickens so that the electronic and ionic resistivities are more balanced. However, the potential measured on the metal is always negative (even though it may sometimes be small) indicating that electron transport is usually the more difficult (and hence rate determining) process.

6. Corrosion kinetics

During the pre-transition period of corrosion (i.e. prior to the accelerated, roughly linear, post-transition period indicating the development of gross porosity) the kinetics at reactor temperature (300–360 °C) have repeatedly shown an approximately cubic rate law, rather than the parabolic law predicted for a process controlled by bulk diffusion of oxygen through the oxide [37]. Analysis of oxygen isotope diffusion profiles [23,43] showed that the crystallite boundary diffusion was more rapid than bulk diffusion, but this should still result in parabolic kinetics if the oxide crystallite size remained constant as the oxide thickened. Electron microscope studies of the evolution of the oxide crystallite structure [13,44–47] have shown that this is not the case. Although the thin oxide films contain many orientations of small roughly equiaxed crystallites [44], as the oxide thickens some of these orientations grow preferentially. This leads to a columnar oxide crystallite structure (Fig. 7) with a strong fibre texture [48]. The driving force for this structural evolution is thought to be the large compressive stresses that develop very early during the growth of the oxide because of the high Pilling-Bedworth (PB) ratio (~1.56) and the lack of zirconium ion migration. Because in most experiments the metal thickness is much greater than the oxide thickness, the oxide is constrained to accommodate the PB ratio largely by growth in the thickness direction. This is not true for very thin specimens, or at very high temperatures, where measurable growth of the metal occurs. Thus, the cubic oxidation kinetics possibly result from the reduction in the crystallite boundary area (at least during the first 1 μm oxide growth), and the variability in the actual

Fig. 7. Columnar oxide crystallite growth on Zr after 24hr in 600 °C air [6]. Oxide-metal interface is at bottom. Micrograph is from a two stage (Formvar/carbon) replica of the oxide fractured (after dissolution of the Zr matrix) by gluing the oxide to a glass microscope slide, scribing the back surface of the slide, and fracturing the composite of slide and oxide.

measured exponent of the rate law ($\Delta l \propto t^{0.33}$) over the range ~0.25–0.37 (Fig. 8(a)) may be ascribed to variability in the development of the columnar crystallite structure. It has been suggested that the increase in the compressive stress in the oxide with increasing thickness [6] can directly affect the oxygen diffusion coefficient by compressing the oxide lattice and thus making oxygen diffusion progressively more difficult [49]. It seems more probable that this would affect bulk diffusion of oxygen, rather than the dominant crystallite boundary diffusion. This conclusion seems to be borne out by the observation that the kinetics are much closer to parabolic than to cubic during high temperature (800 °C) oxidation where the bulk and boundary diffusion coefficients for oxygen become similar, but where the oxide structure is still columnar and high compressive stresses are still present. At these temperatures a significant fraction (~40%) of the oxygen that reacts goes into solution in the metal [6,9], but only at very high temperatures and/or low oxygen pressures does the oxide fail to thicken and the oxidation rate become controlled by oxygen dissolution in the metal.

7. Oxide breakdown processes

In general it is not possible to grow oxide films on zirconium alloys that are thicker than 2 μm without a change in the kinetics to either an approximately linear or a cyclic kinetic stage (post-transition) that is considered to indicate the development of some sort of porosity in the previously protective oxide. Although the pre-transition oxide is regarded as a diffusion barrier this does not mean that it is necessarily perfect. A few small flaws in the pre-transition oxide will not materially affect the diffusion controlled oxide growth kinetics, although they may be important for the cathodic half-cell processes (electronic conduction and hydrogen absorption). These aspects will be discussed later. A much more severe degradation of the oxide by cracking or pore [1] formation is envisaged at the transition in the kinetics. This transition exhibits at least three different modes of development under different conditions. In aqueous solutions at 300–360 °C this transition can be quite sudden (i.e occurs in a time interval that is very short compared with the duration of the pre-transition period), involve a sharp increase in oxidation rate and a successive cycle of apparently pre-transition corrosion periods (Fig. 8(b)) [50].

[1] Pore is used here in its normal meaning in corrosion of a 'canal' i.e. a connected route for molecular transport, and *not* in the connotation of 'a closed void' which is general in ceramics studies. A pore would differ from a crack in its 'aspect ratio'. A crack will have one small dimension and two large ones; a pore, one large one and two small (not necessarily equal) dimensions.

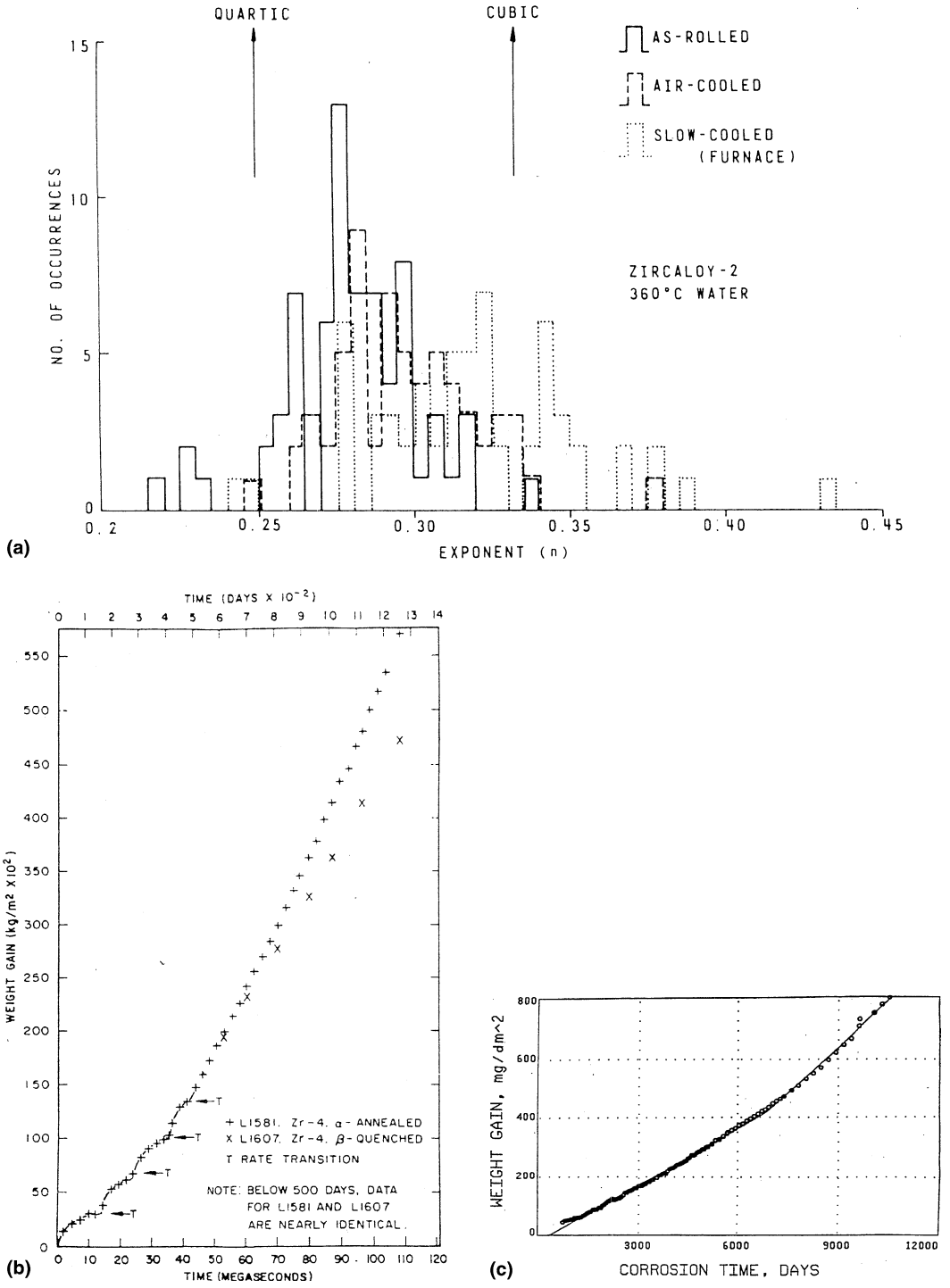

Fig. 8. (a) Histogram of pre-transition oxidation rate exponents (n) [6]. (b) Cylic nature of post-transition corrosion of Zircaloy-4 in 633 K water [50]. (c) Prolonged acceleration of post-transition corrosion after end of cyclic behaviour in 316 °C water [50].

At higher temperatures in oxygen or low-pressure steam (the high pressure steam effect will be discussed later) a more gentle change (i.e. no sharp discontinuity in the kinetic curve) from a cubic to an accelerated linear

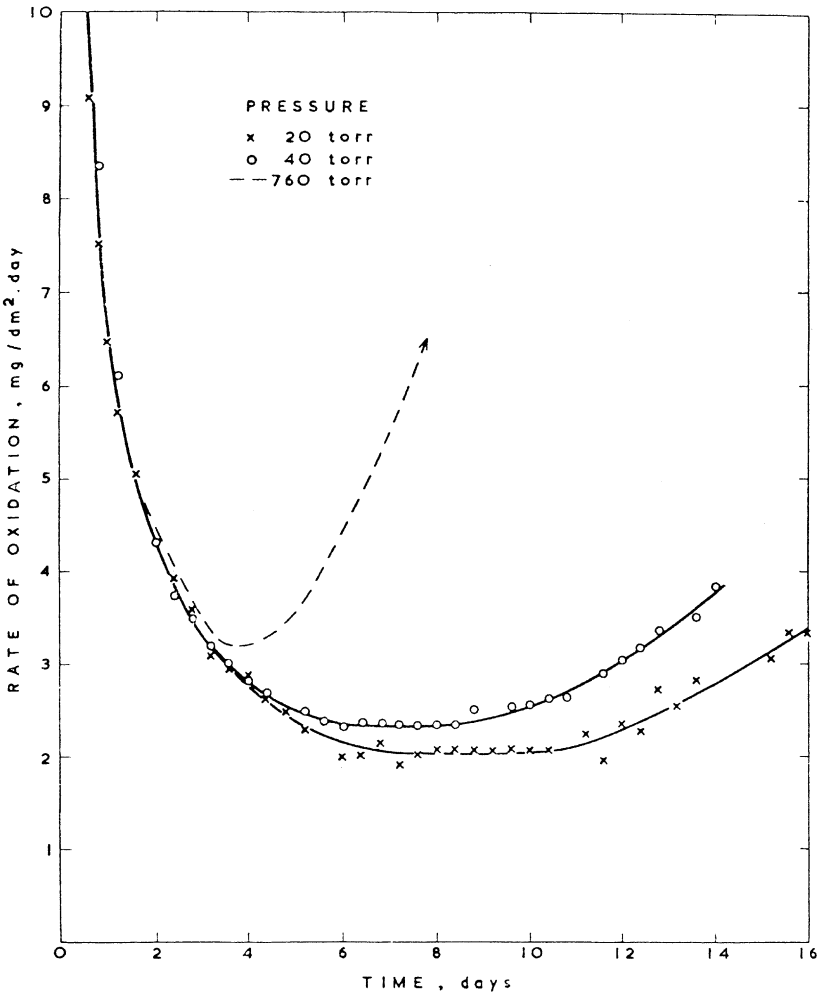

Fig. 9. Effect of pressure on the rate of propagation of the oxidation kinetic transition for Zircaloy-2 in 500 °C steam [51].

corrosion kinetic process is seen (Fig. 9) [51]. This 'gentle' transition process can occupy a time interval comparable to the whole pre-transition kinetic period, in contrast to the sudden breakdown seen in high temperature water. A 'slow transition' may be a fast process nucleating and spreading slowly over the surface, or a genuinely slow but uniform process. There is not usually enough evidence to distinguish between them [6]. However, the combined lengths of the cyclic behaviour, before a relatively smooth post-transition curve appears can be very long. The post-transition curve (Fig. 8(c)) is seldom accurately linear, but continues to show a slowly increasing rate even in the longest autoclave tests that have been performed [50]. The authors choose to fit these data to two successive linear rates but a careful study of the first differential of the data shows that the corrosion rate is smoothly increasing, although at a decreasing rate of increase. The third type of oxide breakdown process is the 'para-linear' one that involves a steady kinetic change from approximately cubic, through parabolic, to linear (Fig. 10) without any actual oxidation rate increase throughout the whole process. This is sometimes, but not always, seen during the oxidation of Zr–Nb binary alloys [52]. The number of data points in Fig. 10 is limited, but there has clearly been no increase in rate as is shown in Fig. 9.

A number of mechanisms have been proposed for the breakdown of the pre-transition oxide film. It seems possible that more than one of these may be operating in any given environmental conditions, and that those that are operating may change according to the particular conditions. Amongst others, the most probable mechanisms seem to be:

(1) Cracking of the oxide resulting from the differential stresses across the oxide. New oxide is formed in compression at the oxide/metal interface, and as each

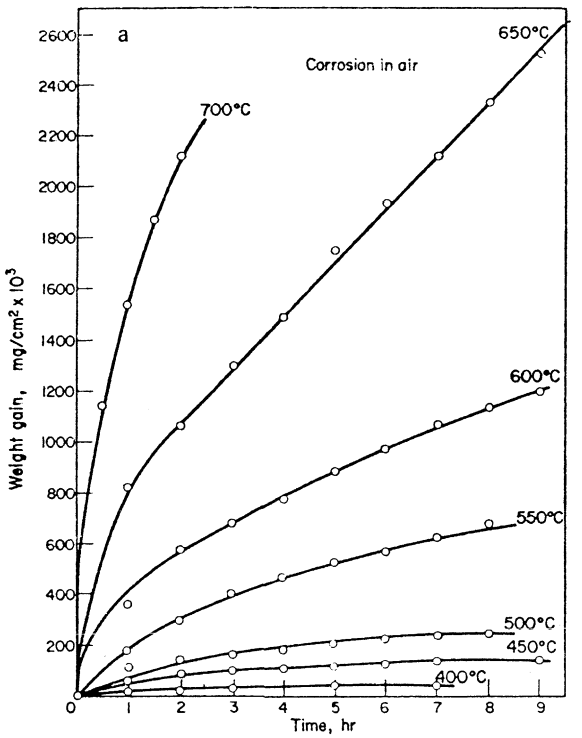

Fig. 10. Para-linear oxidation kinetics for Zr in air at high temperatures [6].

new layer of oxide is formed a balancing increment of tensile stress is applied to the metal surface and to the pre-existing outer layers of the oxide film. Thus, the compressive stress in the oxide is highest at the oxide/metal interface and decreases towards the oxide surface. Eventually as the oxide thickens the stress in the surface layers will become tensile and cracking of the oxide will initiate. However, this cracking should only propagate to the neutral stress axis in the oxide leaving a thick uncracked inner barrier layer [11].

(2) Experiments in which the pressure of the oxidising environment was suddenly changed showed that for oxidations in both oxygen (Fig. 11) and steam (Fig. 12) an immediate change in oxidation rate proportional to the pressure change occurred [6,11], but only after the specimen had passed through transition. During transition the ratio of rates before and after the pressure change slowly rose from ~1 to 4 (the typical pressure increase was ×4). Such a change is possible only if some of the cracks or pores in the oxide propagated right up to the oxide/metal interface. This has been a contentious issue for some time as many investigators who study thin oxide sections in the transmission electron microscope do not see such cracking [53–55]. However, small vertical cracks near to or at the oxide/metal interface can only be seen in the TEM if Fresnel Contrast is used (i.e. taking pictures out of focus, using both over- and under-focus and observing the change in contrast), and

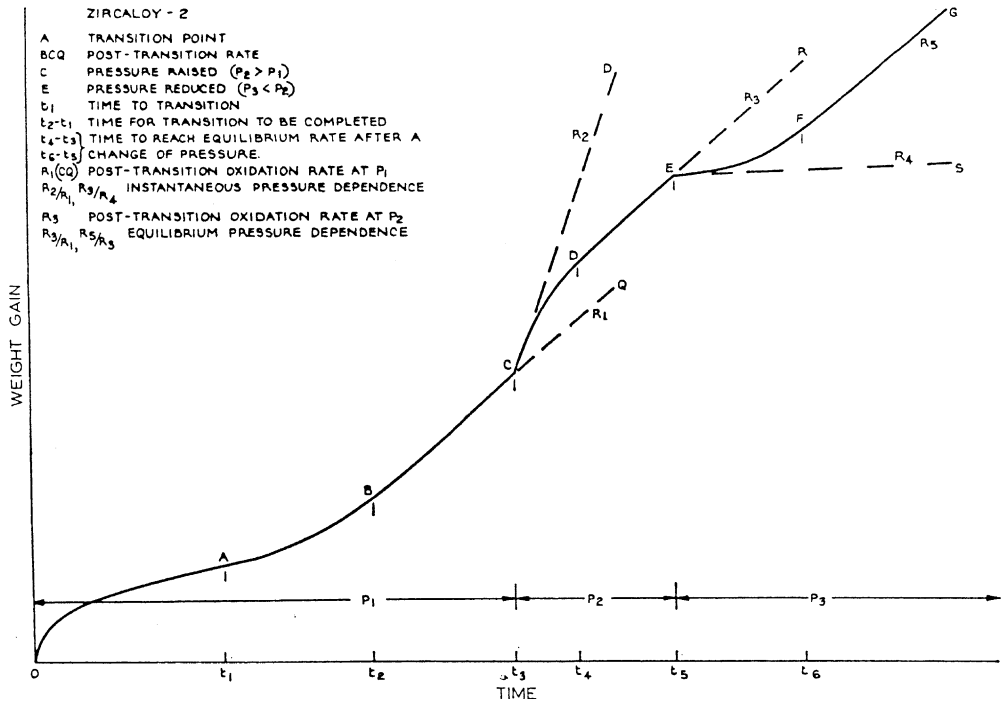

Fig. 11. Oxidation curve obtained by rapidly changing steam or oxygen pressure at <0.1 Mpa [6].

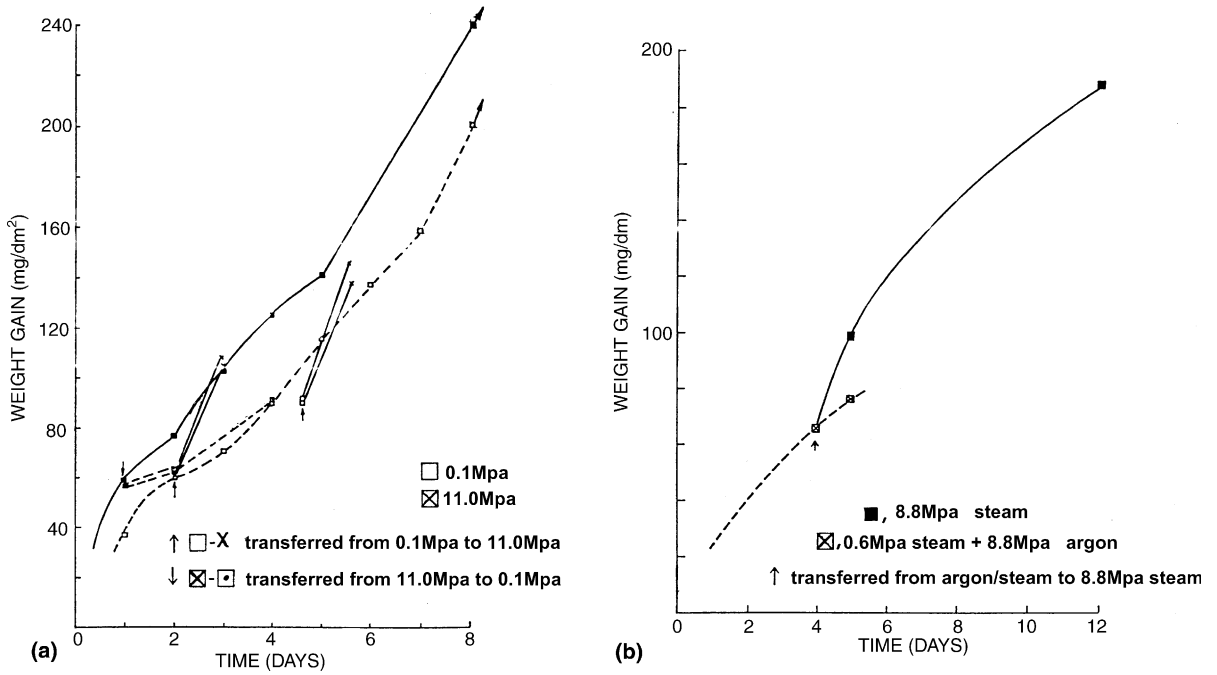

Fig. 12. (a) Weight gain vs. time for Zircaloy-2 'cross-over' experiment (transferred between 1250 psi and 1 atm steam at 500 °C) [19]. (b) Weight gain vs. time for as-rolled Zircaloy-2 in argon/steam; transferred to 1000 psi steam at 500 °C [19].

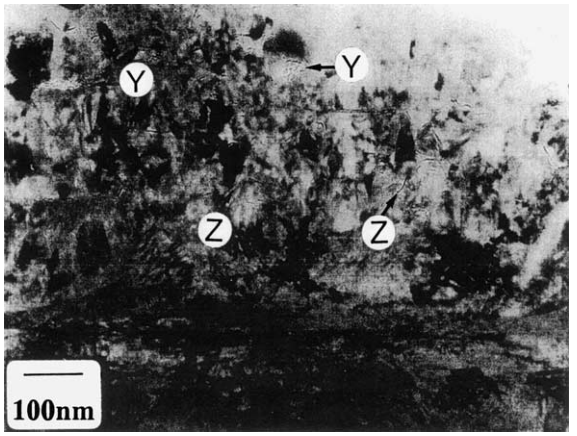

Fig. 13. Overfocus image of section of thin oxide on Zr-2.5% Nb showing cracks at crystallite boundaries (dark lines – Z) penetrating almost to oxide-metal interface (horizontal band just below 'Z' markers) [56].

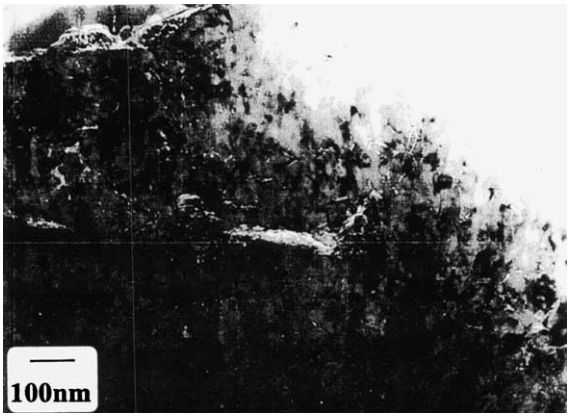

Fig. 14. Underfocus image of section of thin oxide on Zr-2.5% Nb showing lateral cracks only adjacent to the perforation resulting from ion-milling [56].

most investigators seem reluctant to use this technique. Where Fresnel Contrast has been used [56] some small cracks or pores penetrating near to the oxide/metal interface have been seen (Fig. 13). This is further support for the observations during the pressure change experiments, and for the low final resistivities observed in mercury porosimeter studies [11], both of which indicate penetration of cracks or pores very close to the oxide/metal interface. Thus, to explain these a mechanism that can generate cracks in the part of the oxide under compressive stress is needed. The large lateral cracks that are often seen where the ends of columnar oxide crystallites terminate (Fig. 14) may be artefacts resulting from the mechanical cutting and grinding operations involved in preparing sections for examination [57], since they are not seen in oxides not undergoing any cutting or grinding (Fig. 7). The ends of the columnar

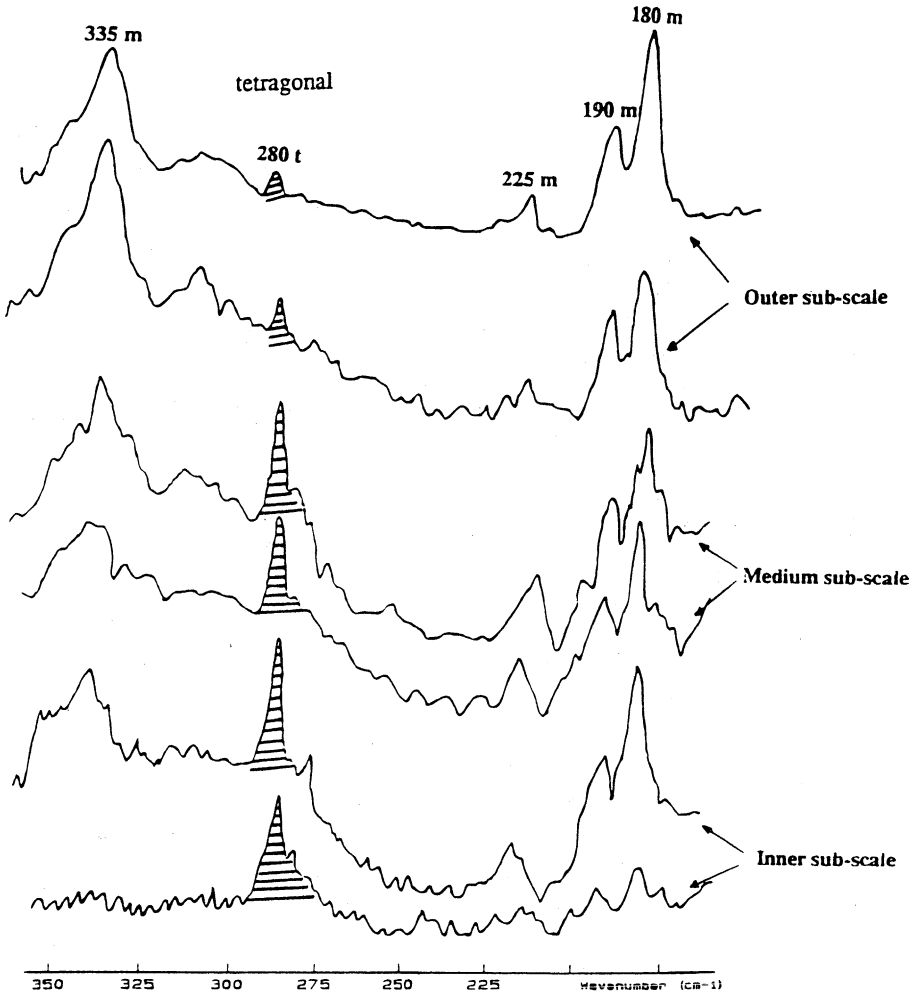

Fig. 15. Raman spectra at different depths of the oxide layer on the Zircaloy-4R after 65 days in steam at 400 °C [58].

crystallites would (of course) represent a plane of weakness in the oxide that could initiate such cracking during sample preparation. A possible breakdown mechanism could result from the transformation of the large fraction of the tetragonal zirconia (t-ZrO_2) phase observed near the oxide/metal interface by Raman spectroscopy (Fig. 15) [11,58]. If the t-ZrO_2 is stabilised by the compressive stress in the oxide then it will transform to monoclinic zirconia (m-ZrO_2) and in zirconia ceramics [59] the shear resulting from twinning during this transformation can result in microcracking [11]. Much less t-ZrO_2 is apparently observed in oxide sections examined in the TEM [60] suggesting that only a small fraction of the t-ZrO_2 was chemically stabilised. However, the texture in the oxide can make it difficult to identify the tetragonal phase. Since the compressive stress in the oxide is obviously relaxed during the preparation of TEM specimens, the stress stabilised t-ZrO_2 would have transformed to m-ZrO_2 during the specimen preparation. But then, of course, the observed crystallite boundary cracks or pores could have formed at the same time. We are left with a dilemma that is very difficult to resolve (another kind of 'Uncertainty Principle'?); how to establish the presence or absence of pores and cracks near the oxide/metal interface without creating the features being sought.

Techniques that can sensitively detect such small features without any preparative operations that could create cracks or pores are limited. Electrochemical Impedance Spectroscopy (EIS) because it averages over a large area, and because it requires matching with an equivalent circuit model containing several components (or layers) has difficulty detecting small numbers of fine cracks [61] and the technique tends to give results affected by the selected model. There have been may recent papers employing EIS techniques, but the insight they give is very limited, and a more extensive discussion of them here does not seem to be justified by space limitations. Mercury porosimetry [62] can detect small

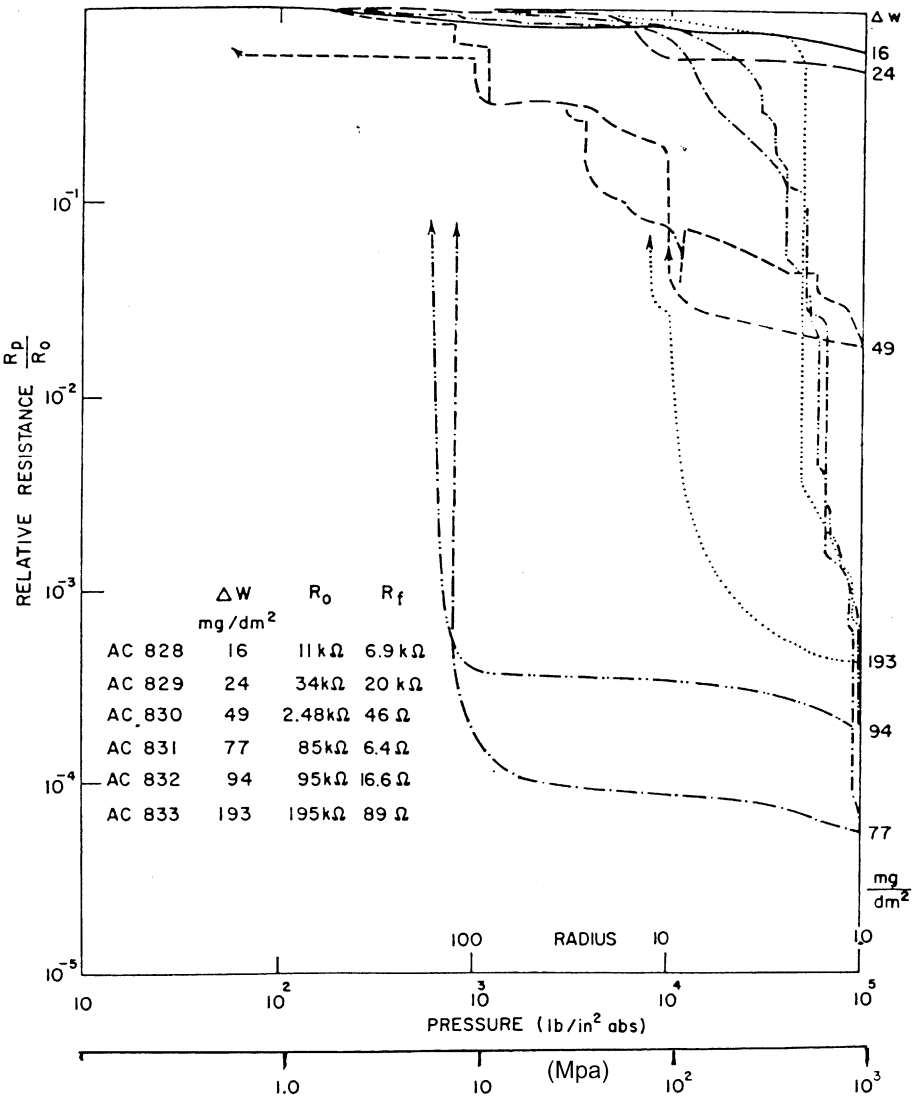

Fig. 16. Porosimeter results for oxide films formed on Zircaloy-2 in 400 °C steam [62].

cracks or pores, if a high enough pressure can be achieved (Fig. 16), but still leaves residual concerns that the high pressure could be creating some of the features that it measures; even though repeated pressurization of the same specimen showed no changes. The dilemma remains!

(3) Chemically stabilised zirconia ceramics undergo degradation from t-ZrO_2 to m-ZrO_2 when exposed to moisture, even at low temperatures ~100 °C [63]. This results in a micro-porous surface layer which grows progressively to depths that are large compared with the usual oxide thicknesses observed on zirconium alloy specimens [64]. This suggests that such a mechanism could progress inwards through the oxide film, eventually reaching the oxide/metal interface. Effects in aqueous solutions have been ascribed to leaching of the aliovalent element (usually Y or Ca) that creates the oxygen vacancies which are the features that allow the oxide lattice to adopt a more symmetrical structure. Although much slower, degradation has been observed even at low water vapour concentrations in air [65]. In these cases dissolution of the stabilising element is not possible and mechanisms based on surface reactions of OH- leading to crack initiation and propagation have been proposed (Fig. 17). Although the later stages of this hypothesis (derived for oxide dissolution in irradiated water) would not be relevant here, the latter mechanism appears to be a possible degradation route for stress

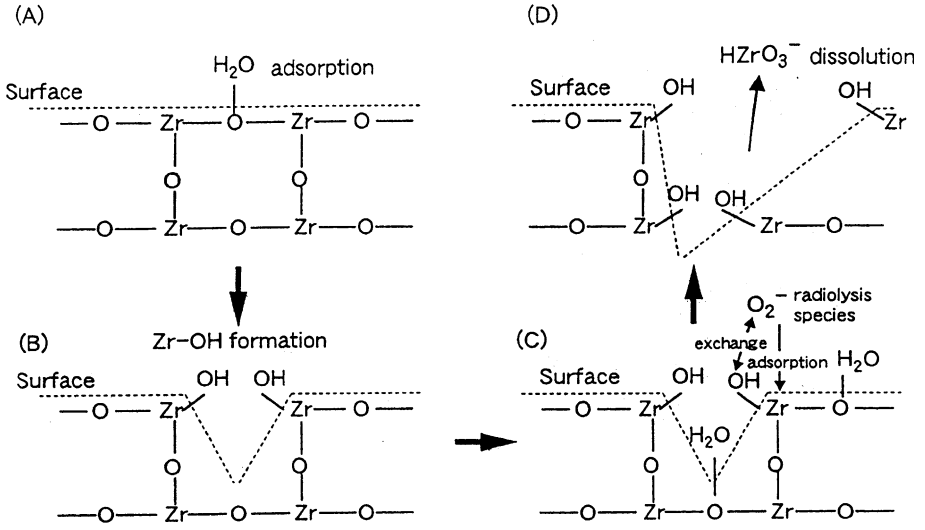

Fig. 17. Model of dissolution process of zirconium oxide into water [107].

stabilised t-ZrO_2 in oxide films on zirconium alloys, while the former mechanism could be applied to areas of the oxide film(e.g. around intermetallic particles) where the t-ZrO_2 could be stabilised by vacancies resulting from aliovalent alloying elements from the intermetallics. At present such a mechanism for oxide film breakdown at transition is plausible, but direct evidence for its operation is lacking. It is not clear even what form such direct evidence might take; the decrease in the t-ZrO_2 fraction in the oxide after transition [66] is compatible with several possible breakdown mechanisms.

(4) The degradation of the corrosion resistance of zirconium alloys in concentrated LiOH solutions has been long known [11,67]. It has been shown that this results from local dissolution of ZrO_2 in these solutions which starts at the oxide/environment interface [11,68,69]. It was initially argued that t-ZrO_2 was being preferentially dissolved from the oxides, as t-ZrO_2 present in oxides formed in water had disappeared after specimens were transferred to LiOH. However, a recent study [68] on zirconia ceramics has found no preferential dissolution of t-ZrO_2 compared with m-ZrO_2. Thus, the porosity generated in corrosion films by ZrO_2 dissolution in LiOH is now thought to be created by attack on the crystallite boundaries in the film. The disappearance of t-ZrO_2 from the oxide films during exposure in LiOH is now ascribed to the degradation process in water noted above (59,64). This may be the best evidence we have that such a mechanism is operating during zirconium alloy corrosion.

(5) The ZrO_2 solubility measured in 1.0 molar LiOH at 300 °C (1.1 ± 0.1 ppb) is very small [69] and the solubility of ZrO_2 in high temperature water would be expected to be orders of magnitude lower than this. On this basis it might be expected that dissolution, even at the oxide crystallite boundaries, would be negligible. However, the alloying elements in the Zircaloys have low solubilities in ZrO_2 and tend to form separate oxide phases. SnO_2 is found concentrated in the oxide crystallite boundaries [70]; Fe is observed as separate crystallites of a mixed iron zirconium oxide in areas close to the intermetallics [71] and chromium has been observed as a Cr_2O_3 phase [72]. There is some slight evidence also for Si segregation at oxide crystallite boundaries, presumably as a thin film of SiO_2 [71]. All of these oxide phases would be much more soluble in high temperature water than ZrO_2. However, all the above studies were carried out on oxides formed in 400 °C steam, and no comparative experiments in 360 °C water have been reported. Experiments in which identical specimens were corroded in 360 °C water, with comparative specimens exposed in 360 °C dry steam, and with the oxides of both studied to establish whether these oxides of the alloying elements are present in both sets of specimens (or not) are badly needed. Nevertheless, the tin content of the alloy has a major impact on the corrosion resistance of Zircaloy type alloys also in 400 °C steam, where dissolution of an SnO_2 phase at the grain boundaries would seem to be impossible. Thus, an alternative to the dissolution of these secondary phases in needed to explain all the observations. The present situation is that we have a number of possible mechanisms for degrading the oxide film at transition, but only [1] has clear evidence in favour of it and this does not help to explain the evidence suggesting that cracks or pores penetrate much closer to the oxide/metal interface than would appear to be possible with this mechanism. Without further critical experiments it is unlikely that further progress will be made,

and without such progress there will continue to be difficulties in interpreting the in-reactor behaviour.

8. Effects of hydrogen

Hydrogen absorption during corrosion in aqueous environments was one of the earliest observations made during the study of zirconium alloy corrosion [3]. The mechanism of hydrogen absorption is more appropriate for a separate review than for this one, but the question of whether or not, and under what circumstances hydrides in the metal phase can affect the corrosion reaction is appropriate for consideration here. The corrosion of solid zirconium hydride in high temperature steam has been studied and was found to be higher than that of the unhydrided metal [73]. Observations on reactor fuel cladding that developed solid hydride 'lenses' at the outer oxide/metal interface [74] confirm this effect of the presence of solid hydride at the corroding interface (Fig. 18). The problem is how to deal with a situation where the hydride at the corroding interface is a two-phase mixture of zirconium metal and hydride. Should the effect be pro-rated by the volume fraction of solid hydride, or is there a lesser effect because of the small oxygen diffusion zone which could prevent hydrides precipitating at the interface. Other work has attempted to address this question [75,76]. The studies by Kido showed increased corrosion starting at quite low average hydrogen contents (600–700 ppm) in 633 K water. However, his micrographs suggested that most of this effect occurred at the edges of his sheet specimens, where the large elongated hydrides lying in the rolling plane emerged at the surface. The patches of thicker oxides on the specimens edges were much broader than the emerging hydride platelets themselves suggesting that whatever breakdown process was being triggered in the oxide by the emerging hydrides was capable of extending beyond the boundaries of the hydride platelets. These patches did not have a lenticular form (like nodular corrosion), but were more of the shape of the oxide filled pits (Fig. 19) that have sometimes been observed with poor water chemistry containing chlorides or fluorides

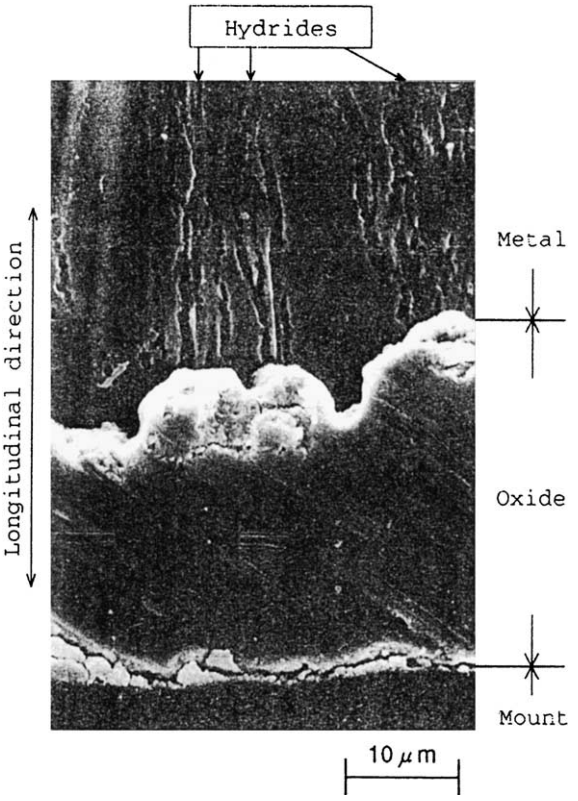

Fig. 19. Scanning electron micrograph of metal–oxide interface at the edge of specimen showing preferential penetration of oxide at hydrides [75].

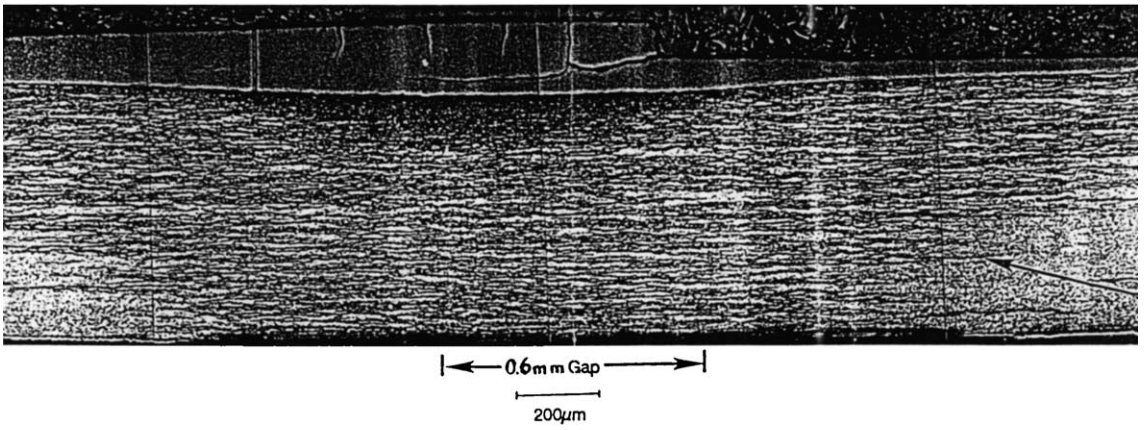

Fig. 18. Acceleration of Zircaloy-4 corrosion by hydrides concentrated at a pellet to pellet gap [74].

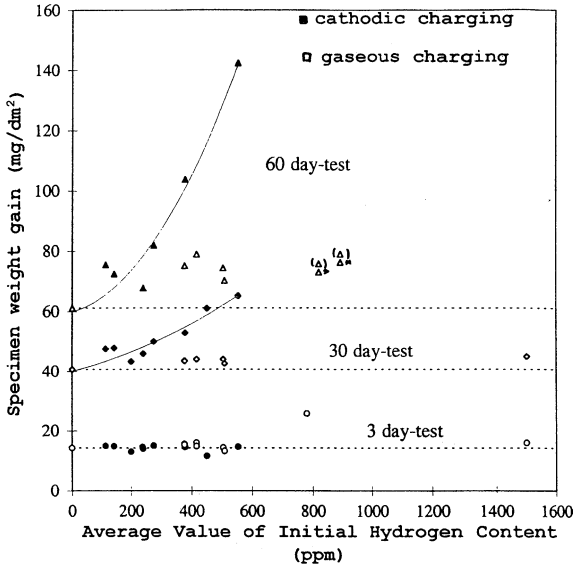

Fig. 20. Influence of the initial hydrogen content on the weight gain of Zircaloy-4 after 400 °C steam corrosion tests [76].

[77,78]. There was no clear evidence for accelerated corrosion on the specimen faces, which the hydrides did not intersect.

The French studies [76], in which sheet specimens were gaseously pre-hydrided tended to show two types of effect. A small positive increment of weight gain that was independent of hydrogen content up to about the solubility of hydrogen at the test temperature (200 ppm at 400 °C) followed by a roughly linear increase in corrosion weight gain at higher hydrogen contents (Fig. 20). The first effect was thought to be a surface contamination effect, although this could not be deliberately replicated, while the second effect suggested that the effect of hydrogen could be directly proportional to hydrogen concentrations above the solubility, even in the two phase ($\alpha + \delta$) region. In this work again metallography did not show a significant number of hydrides intersecting the specimen surfaces, but edge effects were not examined in detail. Thus, no clear conclusions can be reached about how to allow for the presence of hydrides other than in the form of solid hydride layers.

9. In-reactor corrosion morphology

A number of different corrosion morphologies have been observed under irradiation either in test reactors or power reactors.

(1) *Uniform oxide growth* is usually observed in Pressurised Water (or Heavy Water) Reactors provided enough dissolved hydrogen is present to suppress water radiolysis. When these films become very thick ($\geqslant$100 μm) oxide delamination and spalling occur [79]. Some cladding has been observed to spall at lower oxide thicknesses.

(2) *Nodular corrosion* has been a perennial problem in Boiling Water Reactors where water radiolysis and boiling allow oxygen to accumulate in the water. Similar corrosion was observed in the Obrigheim PWR during the first cycle when hydrogen was not added to the coolant [80]. These nodules are usually lenticular in shape and nucleate early in the reactor exposure (1st cycle). Some early experiments in the Vallecitos Boiling Water Reactor produced nodules that were more spherical in shape [81]. This may have been a consequence of the Zircaloy-2 fabrication route, although similarly shaped nodules were produced in a Petten water loop test that was contaminated with chloride [77]. In general, rigorous control of second-phase particle sizes, by adjusting annealing times after a late β-quench, has largely eliminated the nodular corrosion problem [82], although with the consequence of enhanced uniform oxide growth, and sometimes with the late development of nodules (Fig. 21).

(3) *Shadow corrosion* became evident in the BWRs when 'shadows' of the stainless steel control-blade handles were observed on the outsides of fuel boxes (Fig. 22) [83]. However, this was only the most visible observation of the phenomenon. Small patches of thicker oxide appear always to be present at contact points between fuel cladding and spacer springs (stainless steel or nickel alloys) [84], however, the phenomenon only became a problem when a severely enhanced example (Fig. 23) of it occurred in the Liebstadt BWR [85]. It is apparently related to dissimilar metal couples; is closely related to the common nodular corrosion phenomenon, which was observed in early work only under stainless steel not under Zircaloy grids [86]; and has been

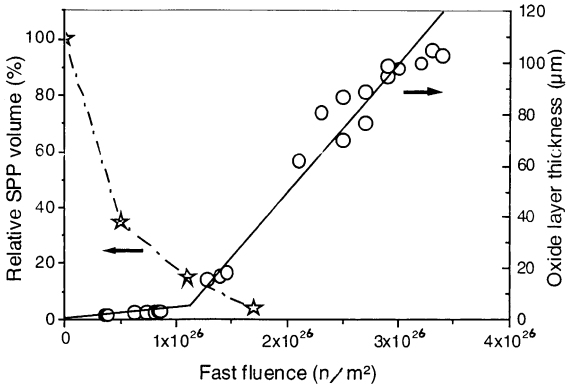

Fig. 21. Influence of irradiation to very high fluences at 290 °C on corrosion and SPP dissolution of Zircaloy-4 with large SPP [ASTM-STP-1423, p. 122].

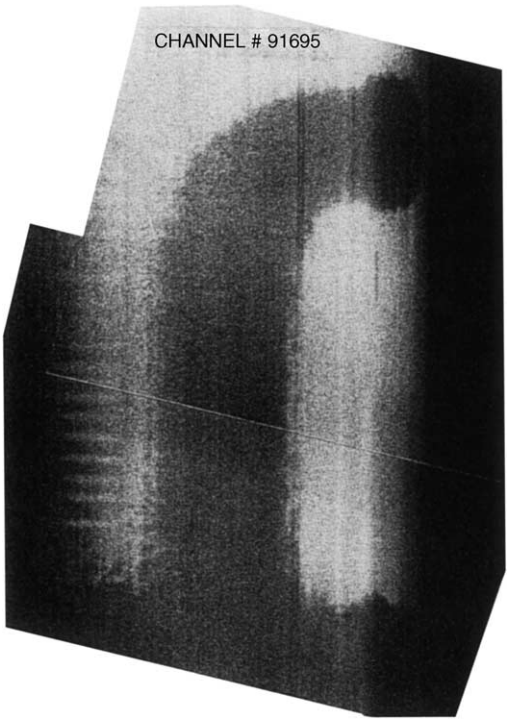

Fig. 22. The shadow of a control blade handle on the adjacent channel [83].

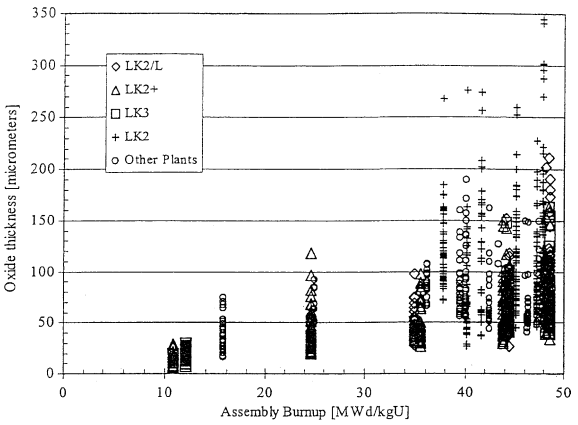

Fig. 23. Maximum spacer shadow corrosion oxide layers measured at KKL in 1999, compared to ABB Atom database from plants operated with iron surplus water chemistry [85].

seen to a minor degree adjacent to welds in Zircaloy-2 and to differently fabricated zirconium alloys [85]. This phenomenon has been extensively studied only recently and its electrochemical component has been confirmed [87]. It is not observed in PWRs with adequate hydrogen additions.

10. Irradiation effects in zirconia films

10.1. Enhanced diffusion

Because the growth of oxide films on zirconium alloys requires the diffusion of oxygen ions through the films it was expected from the start of the exposure of zirconium alloys in-reactors that displacement of ions from their lattice sites by fast neutron or heavy particle (primary knock-on) damage would lead to enhanced point defect concentrations, enhanced diffusion and hence enhanced corrosion in-reactors [88]. Mechanisms similar to those leading to enhanced rate processes in the metal were anticipated [89]. It appeared from results in reactor loops and other oxidation rigs that this was precisely what was happening [9,11]. However, when reliable data from power reactor oxides became available it was evident that there was no irradiation enhancement of the diffusion controlled pre-transition corrosion rates (see later). Transmission electron microscope studies of irradiated oxides from power reactor components showed little or no evidence of the expected radiation damage features (point defect clusters, dislocation loops, voids) [90]. Thus, the inference is that irradiation produced point defects recombine almost completely in oxide films on zirconium alloys. The features in irradiated oxide films, thought to be dislocations were probably twins from the $t \rightarrow m$ ZrO_2 transformation. Proton irradiation of oxide films gave no evidence for these features either [91] and recent studies using Xe ions [92] have found little evidence of radiation damage but did find an array of possible Xe bubbles.

Electron irradiation (10 MeV) of Zircaloy-2 and Zr–2.5Nb [93], produced no visible features in the oxide. Post-irradiation corrosion rates were reduced for Zr–2.5Nb as a result of irradiation enhanced decomposition of β-Zr in the metal phase. (This is also observed following neutron irradiation of the metal). Post-irradiation corrosion rates were unaffected for Zircaloy-2, showing that electron irradiation of the metal is unable to displace Fe from the intermetallics as is the case for neutron irradiation.

These are quite different from the results obtained on other bulk ceramic oxides [94] where the development of micro-voids has typically been the primary result of neutron irradiation. Grain sizes in these ceramic oxides are much larger than in zirconium oxide films, and this may be an important reason for the absence of micro-voids in the latter. The formation of the micro-voids is believed to require sufficient mobility in the interstitial point defects to allow them to migrate to sinks (grain boundaries?). This allows the vacancies to condense to form the micro-voids, perhaps with the assistance of small clusters of H or He atoms [94] and maybe the effect of the Xe ions above [92]. In irradiated Al_2O_3 micro-voids

are formed throughout the $\geqslant 5$ μm grains, and are aligned with the c-axis, whereas in MgAl spinel only a single layer of micro-voids is formed on either side of the grain boundaries. It is thought that interstitial diffusion is so limited in this structure that only within <10 nm of the grain boundaries can diffusion of the interstitials to the g.b. sink occur at 1100 K [94]. In the remainder of the grain volume complete recombination of point defects could then occur. In MgO no micro-voids are observed, and in irradiated stabilised zirconia [95] only small numbers of micro-voids are seen throughout the 3 μm grains.

10.2. Enhanced electron conduction

Zirconium oxide films are good insulators, and the β, γ flux in-reactor would be expected to result in large increases in the electronic conductivity (Fig. 24(a)) [149], as a result of the high production rate of electron-hole pairs and Compton electrons. When zirconia corrosion films were exposed to the electron beam in a 1 MeV electron microscope large increases in conductivity were observed in the beam-on condition, with a rapid return to normal when the beam was turned off (Fig. 24(b)) [96]. Gamma-irradiation measurements of the conductivities of oxide films on Zircaloy specimens using AC rather than DC techniques, showed no effects perhaps because the oscillating potentials encourage electron/hole recombination [97]. The result of neutron irradiation induced redistribution of the alloying elements in-reactor [98] could cause permanent changes in oxide conductivity after long irradiations depending upon the precise form of the displaced atoms and their valence state. For instance, the displaced Fe in the metal phase is often seen to be aligned along features such as c-type dislocations in the metal. Oxidation of such a region could result in an alignment of Fe oxide crystallites that could provide a high conductivity path in the oxide [71]. An immediate effect of gamma-flux on the conductivity of zirconia films would be expected but has not been reported, although direct measurements in a low-flux reactor using a DC technique did show large increases in oxide film conductivity [149].

10.3. Enhanced dissolution of oxide films

The severely accelerated corrosion of zirconium alloys in irradiated $(UO_2)SO_4/H_2SO_4$ solutions was ascribed to a number of mechanisms at different times [5]. One of these involved the enhanced dissolution of regions of the oxide damaged by the passage of fission products [99]. The dissolved material redeposited on the specimen surfaces, or elsewhere in the in-reactor loop. Although this mechanism was subsequently abandoned in favour of one based on irradiation damage in the metal phase, re-examination of electron microscope replicas of Zircaloy-2 specimens exposed to very low fission power densities [100] showed that individual fission fragment tracks in the oxide may have dissolved out, suggesting that enhanced dissolution of fission damage tracks in the highly acidic solutions was a possible explanation.

ZrO_2 is an amphoteric oxide and dissolution in highly alkaline solutions would also be expected. Hydrothermal measurements of the solubilities of ZrO_2 in a range of alkalis (LiOH, NaOH, KOH, NH_4OH) [101] show that the order of the ZrO_2 solubilities matches the order of the effects on the corrosion rates [67]. That the solubility of ZrO_2 in 1 molar LiOH could be sufficient to explain the observed high corrosion rate was shown, and during this study transfer of specimens from low to high LiOH solutions was observed to result in small weight losses on the specimens initially, but followed by a change to a high rate of weight gain typical of the high LiOH concentration. Thus, the dissolution of oxide crystallite boundaries by LiOH (if this is what is occurring) involved the dissolution of only a very small volume fraction of oxide [69]. The protective effect of boric acid, ascribed to plugging of porosity in the oxide by a boron compound [102] has probably prevented the observation of such oxide dissolution in PWRs. The presence of ZrO_2 in crud has been observed, but establishing its origin is difficult. It is uncertain, at present, whether or not these oxide dissolution effects are enhanced by irradiation or not. However, TEM studies of oxides on Zr–2.5%Nb alloy pressure tubes [103] after long exposure (10.6 yr) to primary coolant (containing 3×10^{-4} molar LiOH with no boric acid) found that the outer layers of the oxide had been recrystallised. Similarly large recrystallised oxide grains in films formed on Zircaloy-4 have only been seen on cladding exposed to very severe, non-standard thermal hydraulic conditions [104,105].

Oxide dissolution has also been proposed as a mechanism for enhanced corrosion in BWR water conditions [106], and evidence for reduced weight gains during gamma irradiation in 288 °C water have been presented [107]. This has been matched by evidence for weight losses by bulk stabilised zirconia specimens exposed in similar conditions [29,68]. In these cases the high transient concentrations of hydrogen peroxide have been argued to be the active solvent species. However, the degradation of stabilised t-ZrO_2 in water or water vapour in the absence of irradiation presents an alternative mechanism that would be active in the absence of irradiation, and whose effect is not well understood at present. The pores that are formed appear to propagate almost right up to the oxide/metal interface [108]; are large in number (10^9 cm^{-2}); small in size ~2 nm

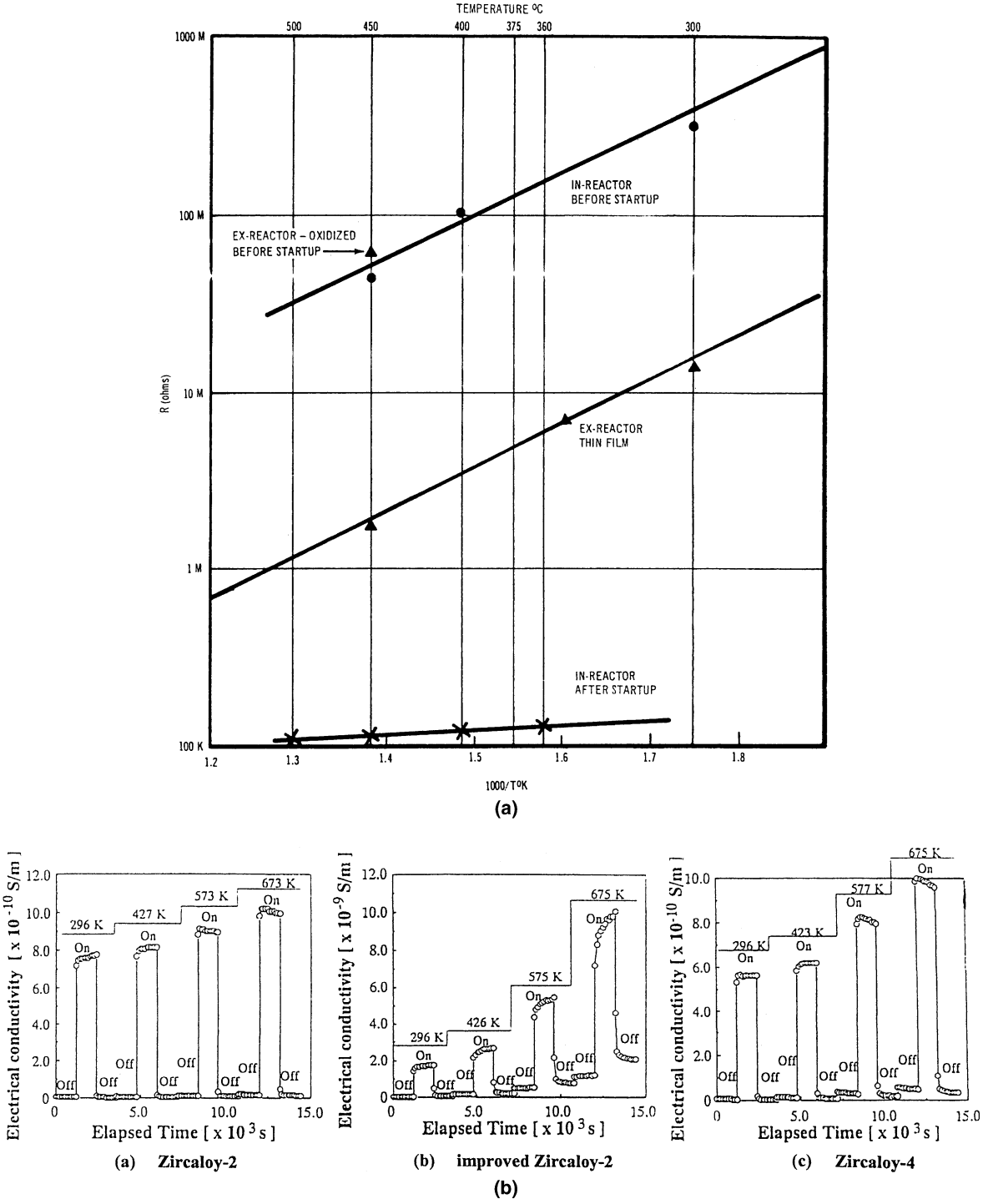

Fig. 24. (a) Log R vs. $1/T$ plot of resistance of ZrO_2 film on Zircaloy-2 in-reactor [149]. (b) Time dependence of electrical conductivity for zirconia films under irradiation with a 1 MeV electron flux of $1.4 \times 10^{18} e/m^2 s$ with beam on and off [96].

diameter) and represent a volume fraction of the oxide (0.001) that is very similar to the volume fraction of crystallite boundary pores/cracks observed by Ploc and Newcomb [56].

10.4. Irradiation induced phase transformation in ZrO_2

An irradiation induced phase transformation from monoclinic to cubic ZrO_2 during irradiation with fission fragments was proposed [109] as the degradation mechanism during irradiation in uranyl sulphate solutions where oxides were observed to be largely cubic ZrO_2 [5]. It was shown that this effect was predominantly a chemical stabilisation of the ZrO_2 by uranium ions. Since there was other evidence that these oxides had undergone a dissolution and reprecipitation cycle [5], reprecipitation from a uranium salt solution would have been a very efficient mechanism for producing such chemically stabilised oxide films. Recent studies of the m → t-ZrO_2 transformation have shown that it can be achieved 'in vacuo' with heavy ion irradiations at room temperature [92,110,111] and is argued to be an effect of the point defects introduced by the bombardment and the strain fields associated with them. However, the authors took no precautions to prevent sputtering of other species from their equipment into their specimens and in one instance deliberately coated the specimens with carbon. The metastable t-ZrO_2 reverts to m-ZrO_2 on annealing in 573 K (300 °C) air (of uncontrolled moisture content). This seems to be rather a low temperature for point defects to anneal out and the effect may have resulted from the degradation by water vapour cited above [63–66], and suggests that such a phase transformation will not occur in water reactors. As we have seen above in PWRs and BWRs the evidence is that the reverse transition t → m-ZrO_2 is occurring. No evidence for a higher percentage of t-ZrO_2 in irradiated oxides from water reactors has been reported.

A study of the effect of trace uranium impurities (0.1–24 ppm) in Zircaloys on the corrosion resistance in 330 °C water in an in-reactor loop showed pre-transition corrosion rates accelerating with uranium content (Fig. 25), but decreasing post-transition corrosion rates (Fig. 26) [112]. No effect was seen on out-reactor corrosion rates. The authors used the Wittels and Sherill reports of a fission fragment induced m → c-ZrO_2 transformation without referencing the evidence for flaws in these studies [5] or showing that there was a high proportion of c-ZrO_2 in their oxides. No details of the loop water chemistry conditions were given and this may have been critical.

10.5. Irradiation induced redistribution of alloying elements

Although strictly speaking an irradiation effect in the metal phase, fast neutron irradiation redistributes the alloying elements (by a primarily knock-on effect) [113] from the intermetallic particles into the surrounding α-Zr matrix [98,114]. The smallest particles dissolve completely, and the largest are significantly reduced in size.

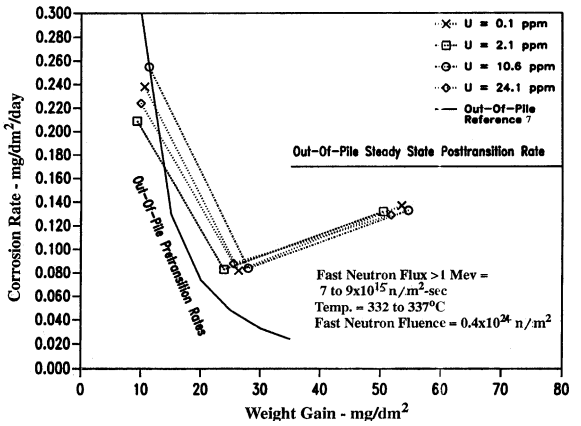

Fig. 25. Effect of natural uranium impurities on in-pile corrosion rate of Zircaloy-4 at 332 °C and very low flux [112].

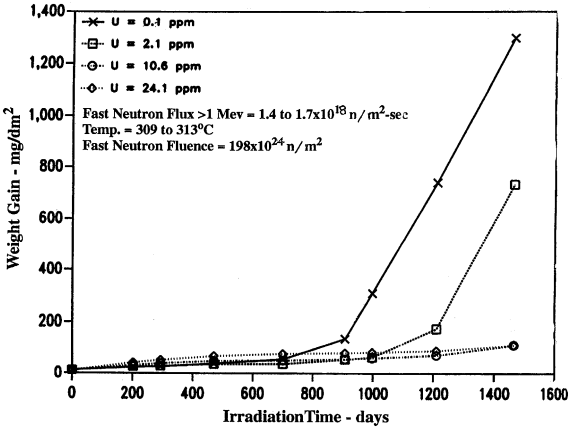

Fig. 26. Effect of natural uranium impurities on in-pile corrosion rate of Zircaloy-4 at 310 °C and high flux [112].

Once displaced from the intermetallics the ultimate location of the Fe is determined by thermal diffusion effects in the vicinity of the intermetallic where c-type dislocations may have formed. Post-irradiation [115] corrosion of such specimens shows progressive degradation of the post-transition corrosion rates with increasing dose (Fig. 27).

11. Galvanic effects in-reactor

In order to see galvanic effects between dissimilar metals a potential difference and an electrically conducting path between the two metals are necessary. In the case of zirconium alloys out-reactor even the 'air-formed' oxide film present on all zirconium surfaces in aqueous environments has sufficient resistivity to prevent significant galvanic currents passing to dissimilar

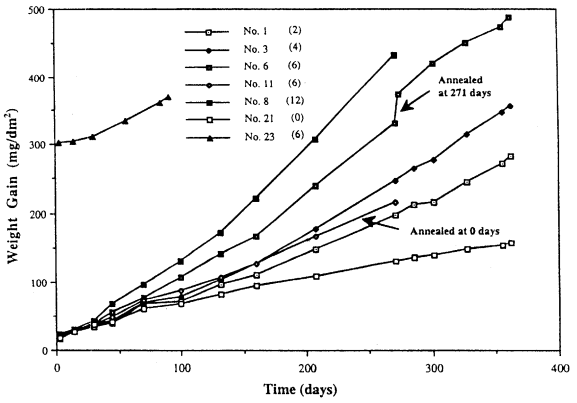

Fig. 27. Corrosion of Zircaloy-2 in 400 °C (673 K) steam. BWR water rod materials irradiated at 288 °C (562 K). Fluences are given in parenthesis (units of 10^{25}n/m^2, >1 MeV) [115].

metals. In-reactor it was learned very early [116,117] that this was not the case when Zircaloy-2 flow-tubes in the K-East Reactor (KER) at Hanford failed as a result of gross cathodic hydriding at ~50 °C as a result of contact with aluminum clad shield plugs in the ends of the tubes. Surprisingly thick interference coloured oxide films were also seen on the Zircaloy tubes, despite the low temperature [128]. Neither of these two effects could be simulated in laboratory experiments because of the resistive oxides on both the Zr and Al components [118]. It was clear that in-reactor either β and/or γ irradiation was increasing the conductivities of both oxide films to the point where galvanic effects became possible.

In a more recent occurrence of the same phenomenon [100], both the development of hydride layers (Fig. 28) and the simultaneous growth of interference coloured oxide films (Fig. 29) on Zircaloy-4 irradiation-growth specimens were monitored after the exposure in the ATR at ~50 °C of the test samples (contained in aluminum specimen holders). A change to Zircaloy specimen holders eliminated the cathodic hydriding process, but not the enhanced interference-coloured oxide growth. This observation of simultaneously enhanced cathodic (hydriding) and anodic (oxide growth) processes was initially puzzling. However, if the growth of the interference-coloured oxides is initially prevented only by the electronic resistance of the surface films, and this resistance was significantly reduced under irradiation then the observations became understandable. The oxide growth is driven entirely by the free energy of oxidation once the rate limiting electronic resistance is reduced, and this oxide growth is only slightly inhibited by the cathodic polarisation of the specimens when in contact with aluminum. The experiments [100] were not continued long enough to observe whether or not the growth of the interference-coloured oxides reached a limiting thickness (Fig. 29); just as in the laboratory the growth of the air-formed oxide on a chemically polished surface reaches a limit of ~2 nm when electron transport through the oxide becomes impossible [7,13,14,120]. The enhanced growth of the interference coloured oxide could be simulated in the laboratory by irradiating anodically

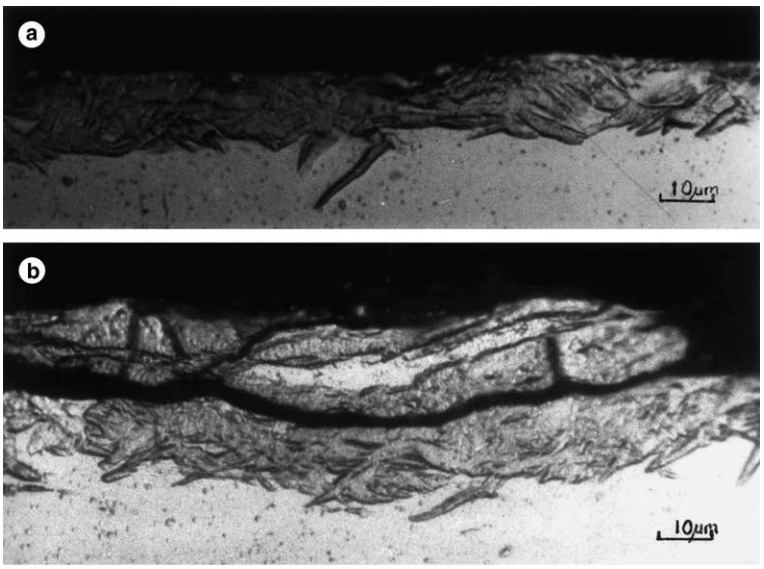

Fig. 28. Hydride layers formed a Zircaloy-4 sheet specimens in Al specimen holders in the ATR core at ~50 °C. (a) Thicker hydride on cut edges than on specimen faces. (b) Most severe hydride formation observed [100].

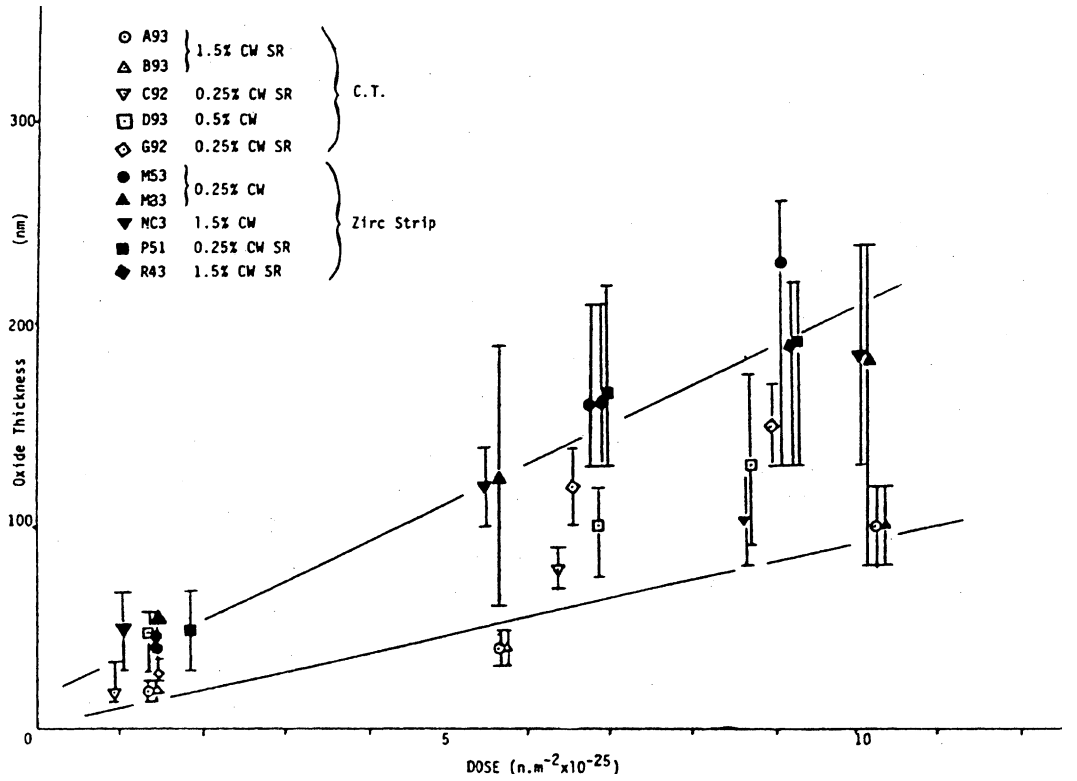

Fig. 29. Formation of interference coloured oxide films on Zircaloy-4 sheet specimens in Al specimen holders in ATR core at ~50 °C. No oxide film growth is observed at this temperature in the absence of irradiation, without anodically polarizing the specimens [100].

polarised specimens with UV light [100]. Theoretically this should require light with a photon energy greater than the ZrO_2 band gap energy, however, photoconduction in zirconia anodic films has been reported at lower energies than this, perhaps because of the impurities such as iron that are more easily ionised than zirconium [119]. Potentially, therefore, the effects of Čerenkov Radiation should be considered for in-reactor effects. These observations could have consequences for the development of 'shadow corrosion' phenomena, although, because of the limited penetration of UV light into ZrO_2 films it could only operate in the early stages of oxide growth.

That a galvanic corrosion component could occur in-reactor, but could not be simulated in the laboratory was known from the early observations of nodular corrosion in reactors [121]. Many subsequent examples resulting mainly from the close proximity of stainless steel or Inconel components have been observed [83,84] but in most instances the excess corrosion resulting from this phenomenon was small, and so it received little attention. However, the basically galvanic nature of the severe shadow corrosion in Leibstadt was confirmed by the absence of any increase in hydrogen uptake under the very thick shadow corrosion oxides. The cathodic hydrogen evolution process had apparently been transferred to the dissimilar metal surfaces [85]. It was evident that other factors than the galvanic couple were important in the severity of the observations. Susceptibility of some batches of cladding was one factor [85,122], but it also appeared that the dissolved iron content of the reactor water was also a factor [123]. In a galvanic corrosion process the conductivity of the electrolyte (water impurities) is obviously a factor in determining the maximum galvanic current that can be passed for a given potential difference between dissimilar metals. The potential difference available will also be affected by the water chemistry. As far as the Fe content of the coolant was concerned the conductivity differences between waters with adequate Fe contents, and those without, was insufficient to explain the magnitude of the effect in KKL. Some more specific effect of Fe, or its chemical form, must be sought. The electrochemical potentials of metals in reactor waters is determined largely by the oxygen content. This accounts for the common observations of shadow phenomena in BWRs. In PWRs with high dissolved hydrogen contents all metals tend to show potentials close to the reversible hydrogen potential [124], so that there is no potential difference to drive galvanic corrosion phenomena in PWRs, and hence no shadow corrosion.

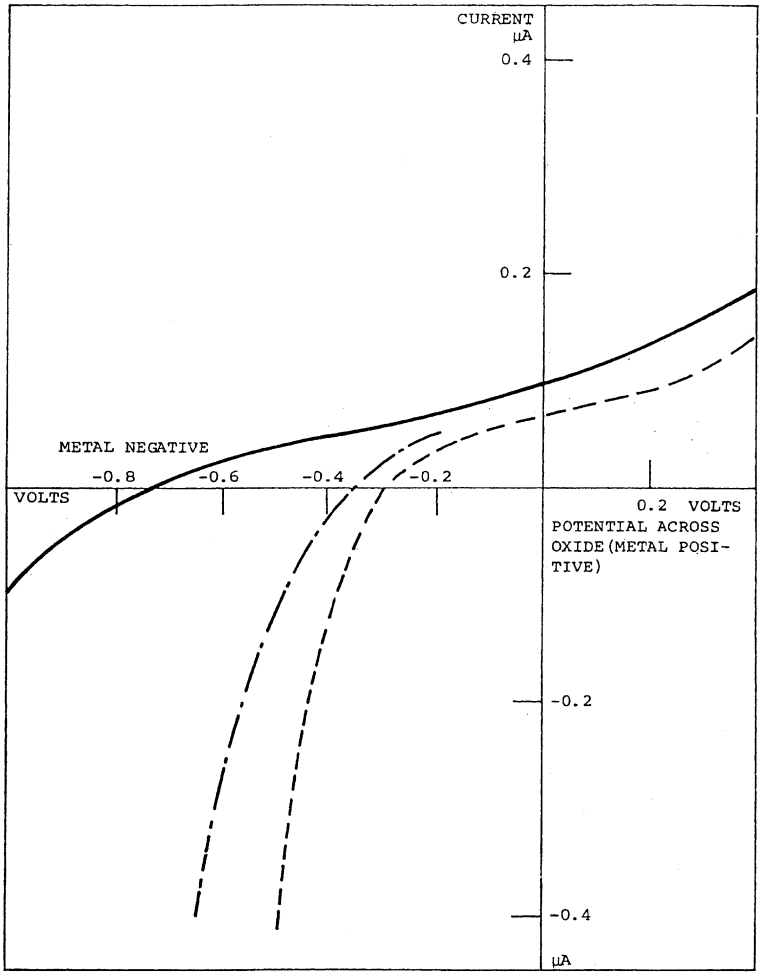

Fig. 30. *I–V* curves obtained in molten salt at 175 °C for a 30 nm anodic ZrO_2 film on crystal-bar zirconium. ----- coated with ~ 10 nm Fe_2O_3 over ~ 10 nm Fe_3O_4; ·-·-· coated with an Fe_3O_4 film crystallised from 300 °C water containing $Fe(OH)_2$; ____ no coating. Specimen area 8.5 cm^2 [100].

If the Fe content of BWR water does not materially affect either the conductivity of the water, or the electrochemical potentials of the dissimilar metal couples, what aspect of the shadow corrosion phenomenon could it have a major impact on? For this to happen it should be remembered that iron oxide deposits on zirconium oxide surfaces had a big effect on the electronic conductivity of the oxide (Fig. 30), depending on the iron oxide being in the right chemical form [36]. The effect depended on the matching of the band gaps of the chemical form of iron oxide on the surface with the band gap of the ZrO_2. When the right combination of band gaps was present electron-hole injection from the iron oxide enhanced the Schottky conduction process through the oxide by factors of up to 20, an increase large enough to explain the severely enhanced shadow corrosion in KKL if the water chemistry had modified the crud deposits in contact with the zirconia surfaces so as to achieve the required band gap matching.

Initial explanations of shadow corrosion [125] blamed β-emissions from the dissimilar metal components of the couples with Zircaloy. This explanation failed with the small shadow effects seen with different zirconium alloys, and with welds [87]. Calculations subsequently showed that such β-emissions did not significantly change the β-background in-reactor [126]. Experimental studies in the MIT water loop confirmed that β irradiation from the dissimilar metal was not a contributor [87,127], showed that galvanic effects were a major contributor (Fig. 31), but did not eliminate the background β as a contributor to the increased conductivity of the zirconia films [96]. The effect of the SPP size in the susceptible batches of cladding may again be an effect on the electronic conductivity of the oxide,

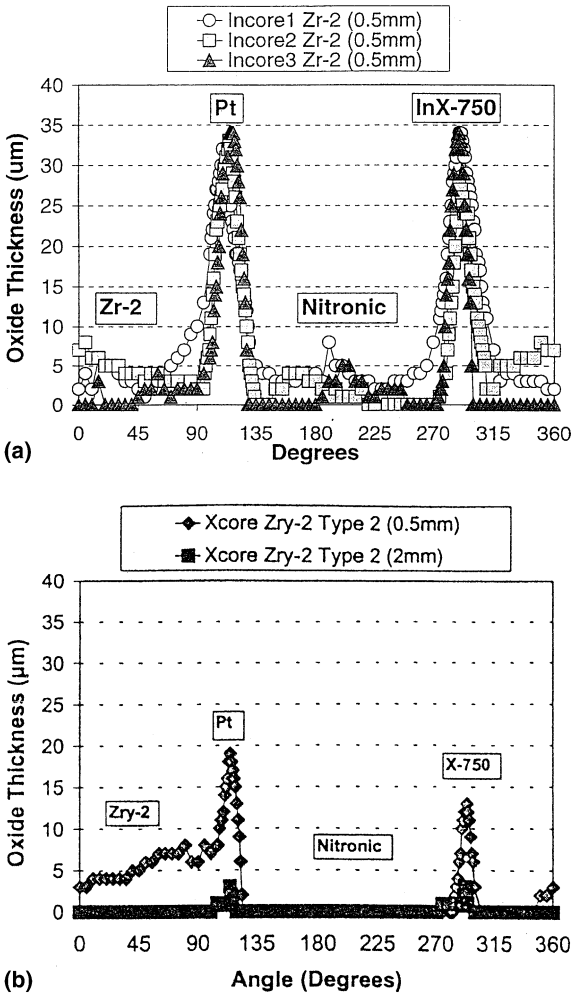

Fig. 31. (a) Oxide thickness measurements on Zr-2 cladding at different elevations (1, 2 and 3) in the core and with four different counter electrodes at the positions indicated (49 days in MITR-2) [127]. (b) Oxide thickness measurements on a similar set of specimens out of the reactor core, but with direct gamma ray shine up the loop flow tube [127].

since small precipitates dissolve most rapidly during irradiation and will dope the oxide with transition metal ions which may enhance the conductivity in regions of the oxide where they are ionized [98].

The prevalence of shadow corrosion effects in water without a high dissolved hydrogen content raises questions about other circumstances where their presence has not previously been considered. Johnson et al. reported shadow corrosion from specimens with platinum implants [128]. Was there a galvanic contribution to all the corrosion rates in these loop tests, since the samples were mounted in stainless steel specimen holders, and none of the tests contained high dissolved hydrogen? Could this same situation have applied to other loop tests where we know little about the specimen holders or the water chemistry [129]? Results for corrosion and hydrogen uptake as a function of reactor water chemistry (Fig. 32) [9,11] show that CANDU reactors, which typically operate with 1–10 cc/kgD_2 are in the cross-over region between typical BWR and PWR in-reactor effects. Thus, it is probable that more than 10 cc/kgH_2 in reactor water would be needed to eliminate shadow corrosion phenomena. This argument is supported by the observation that whether the enhanced corrosion of Zr alloy pressure tubes in the crevice between the CANDU pressure tube and the stainless steel end-fitting (Fig. 33) is a shadow corrosion or a crevice corrosion phenomenon the cathodic process (deuterium evolution) is occurring on the stainless steel, and the pressure tube is the anode in the system [130]. This suggests that, while shadow corrosion phenomena are not seen in PWR water chemistry conditions, they are evident in CANDU water chemistry. Thus, dissolved hydrogen greater than 10 cc/kg water may be necessary to ensure that all circuit materials are performing at the reversible hydrogen potential, and that there will be no potential differences between dissimilar metal couples to generate galvanic corrosion currents.

12. Corrosion rates and oxide morphologies in commercial reactors

With the advent of eddy current oxide thickness measurements [11] an explosion of available data on oxide thickness measurements in both PWRs and BWRs has become available. Only in BWRs are major corrections to the 'lift-off' measurements necessary if magnetic crud deposits are present [131].

12.1. Corrosion in PWRs

It was long maintained by Westinghouse [132] that the uniform oxide thicknesses seen in PWRs could be explained entirely on the basis of thermal-hydraulic conditions, without any enhancement of corrosion from the direct effects of irradiation. This appeared to be at variance with the results of in-reactor loop tests in non-boiling conditions that almost universally showed in-reactor corrosion accelerations [128,129]. The inadequate hydrogen additions to the water (where these are known), that would have been insufficient to eliminate shadow corrosion effects, and the proximity of stainless steel specimen holders, or flow tubes, in many tests, leaves the interpretation of the enhanced corrosion results as direct effects of irradiation in some doubt. With the advent of high outlet temperature, high power density cores in PWRs it appeared that this anomaly between loop test and power reactor data had been eliminated [133]. However, even in the presence of extensive

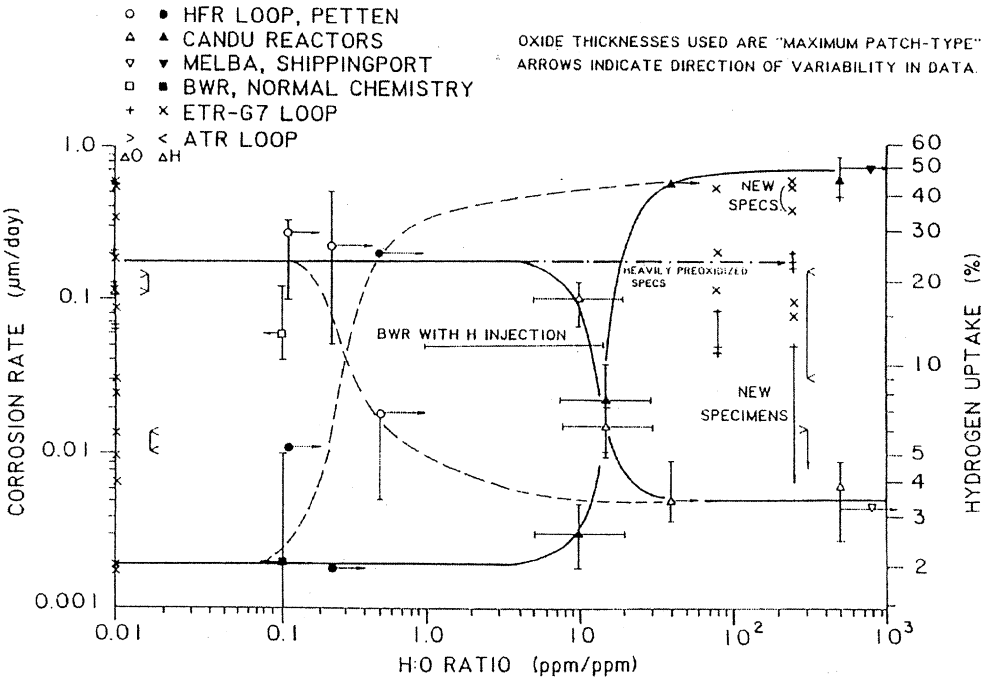

Fig. 32. Effect of water chemistry on corrosion and hydriding of Zircaloy [9].

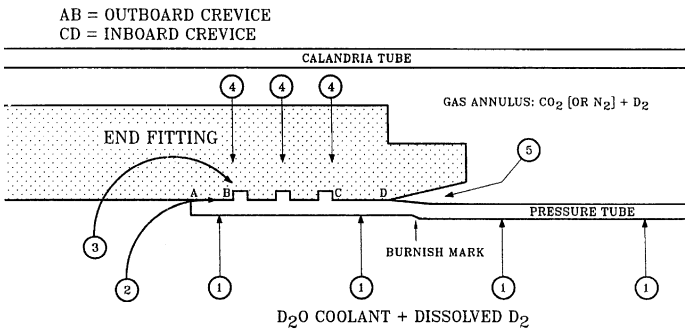

Fig. 33. A schematic diagram of the rolled joint in a CANDU reactor showing the five possible routes originally proposed for deuterium ingress into pressure tubes at rolled joints [130].

sub-channel boiling (Fig. 34), and potential LiOH concentration, if the boric acid concentrates to the same extent as the LiOH, there should always be enough boric acid present to prevent any adverse effects on the corrosion rate [134] except at the end of a reactor cycle. It has been shown out-reactor that concentrated LiOH increases the corrosion rate by generating increased porosity, probably by some dissolution of the crystallite boundaries [69], and that boric acid is volatile in steam and improves Zr alloy corrosion resistance by plugging porosity in the oxide [19] and appears to do the same in high temperature water [69]. Presentation of Siemens data, which had previously been interpreted in terms of in-reactor (irradiation?) factors ranging from 2× to 4–5× from reactor to reactor [135], in terms of normalised time/temperature plots (Fig. 35(b)) appeared to eliminate these reactor related factors [136] and should have allowed for the temperature gradient across the oxide films on fuel at different heat ratings. Despite the scatter in the in-reactor data there appeared to be no in-reactor acceleration in corrosion (over and above that explicable by purely thermal hydraulic factors) until an oxide thickness in excess of ~5–6 μm was reached. From then on a definite acceleration in-reactor, when compared with out-reactor post-transition data, was evident. This way of plotting the PWR data brings them much more in line with the Shippingport observations which clearly show a departure of the irradiated and unirradiated data

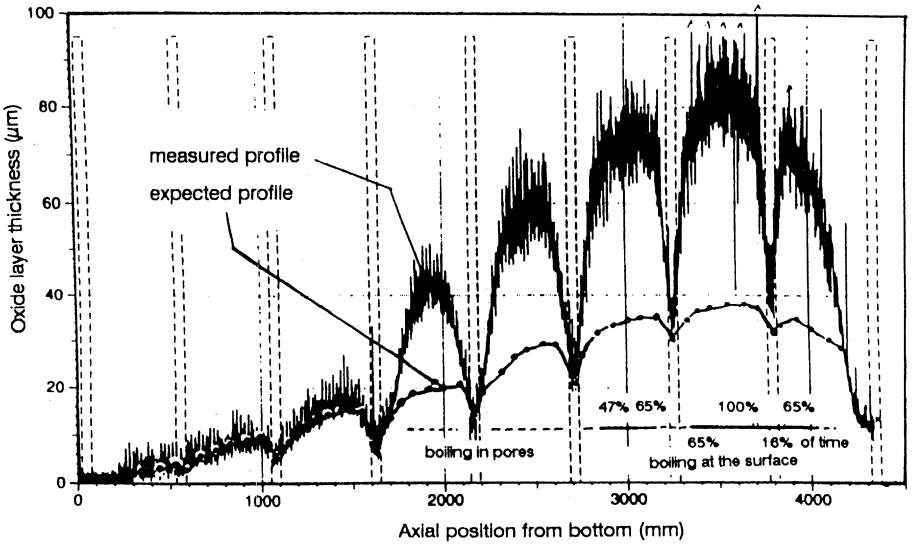

Fig. 34. Accelerated corrosion of a fuel rod exposed for 2 cycles in PWR-H [133].

at 2 μm and suggest that irradiation is accelerating only the oxide breakdown processes and not the diffusion controlled growth of the initial oxide film (Fig. 35(a)).

It is not possible to conclude, on the basis of present evidence, which of the oxide degradation processes discussed above are the primary mechanisms of this in-reactor acceleration of post-transition corrosion. Those most probably involved are the redistribution of the alloying elements as a result of irradiation [90,104,115,137] and (once oxide spalling begins) the formation of 100% solid hydride layers at the oxide/metal interface [74]. Concentration of LiOH in the porous oxide film seems unlikely to contribute, unless rapid oxidation occurs at the end of a reactor cycle (when boric acid is depleted) since no evidence of boric acid depletion in the oxide is found under severe boiling in out-reactor loop tests [138]. However, such periods are very short, and the heat flux of the fuel will be low at the end of the cycle so that boiling should be minimal. These conclusions seem to be supported by the observations that new alloys with improved in-reactor corrosion resistance either have no $Zr(Fe/Cr)_2$ intermetallics [139], or have a different, more radiation stable intermetallic phase [140]. All have low, or no tin additions [141]. This suggests that eliminating the SnO_2 second phase in the oxide [70] is also important. In addition niobium based alloys seem to show much lower hydrogen uptakes, and, hence, do not form 100% solid hydride layers at the oxide/metal interface late in life in-reactor.

Instances of through wall corrosion failures in recent PWR incidents [142,143] have usually been on new fuel, early in its first cycle, with severe crud deposition and recent elimination of boric acid hide out (Axial Offset Anomaly). They appear most like local dry out failures, and evidence for the occurrence of locally high temperatures in the cladding should be sought. Some measurements of Li and B in the oxide films adjacent to the corroded out area of fuel cladding would aid interpretation of these results. A recent report of a through-wall oxidation failure in highly rated fuel without excessive crud or overpowers due to AOA elimination [155] suggests that boric acid concentration may not be as efficient as LiOH concentration in the oxide film under such conditions. Transmission electron microscope studies of the oxides on cladding which had survived such conditions, but with significantly enhanced corrosion, have shown large, equiaxed ZrO_2 crystallites, possibly resulting from hydrothermal re-crystallisation [104,105,144,145]. Similar large crystallites on oxides on the inside of CANDU pressure tubes have been observed after $\geqslant 10$ years exposure [103]. Here there was no heat flux, or boric acid in the dilute LiOH coolant.

12.2. Corrosion in BWRs

Unlike corrosion in PWRs, exposure in BWRs did not result in oxide films that were uniform. The early appearance of small circular areas of thicker oxide (nodules) [81] was characteristic of all zirconium alloy components (not just fuel cladding) exposed in boiling water, where water radiolysis and partitioning of the H_2 and O_2 during boiling resulted in coolants with an excess of dissolved oxygen. Similar nodular corrosion was also observed in reactors with non-boiling water if dissolved hydrogen was insufficient to prevent water radiolysis [80]. Nodules could not be produced in laboratory tests in water at ~300 °C, however, a good simulation of the nodules was obtained in $\geqslant 500$ °C steam at

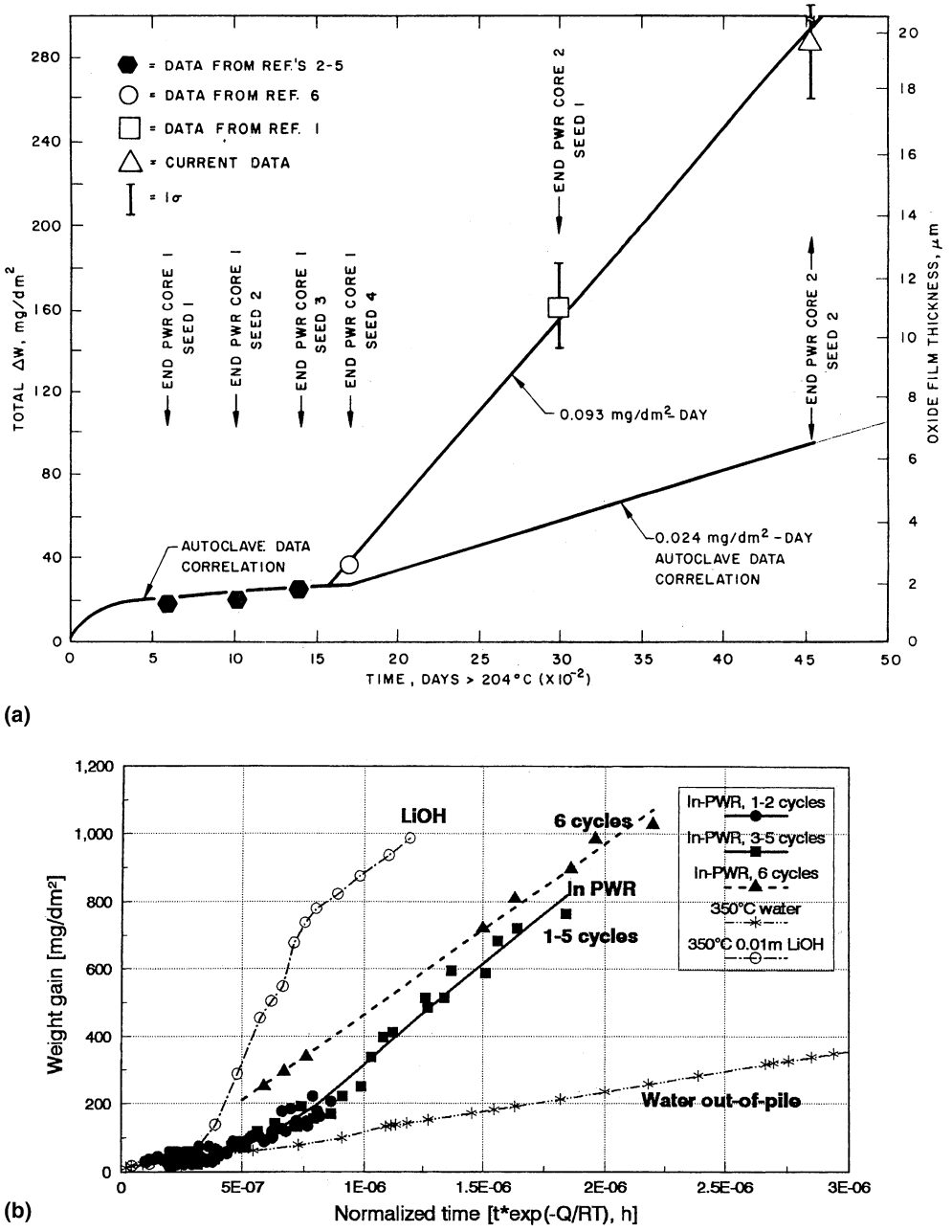

Fig. 35. (a) Total weight gain as a function of exposure time for Region 2 of Rod 11 from Bundle 0120 [9,11]. (b) Corrosion of Zircaloy-4 in PWR in deionized water and in LiOH [136].

high pressure [11]. While such steam tests have been very useful for the laboratory testing of batches of alloys for susceptibility to nodular corrosion in BWRs, it is not clear that the mechanisms operating in these tests are precisely the same as those operating in BWRs. Obviously the primary contributory factors must be the same in each case, and these appear to be those factors related to second phase particle size (Fig. 36) [146]. At the low end of the precipitate size range the increased in-reactor corrosion is enhanced uniform oxide growth related to SPP dissolution in the matrix (Fig. 21) [122]. The necessity for temperatures at or above 500 °C to get good comparisons in laboratory testing may be related to the temperatures needed to get rapid redistribution of the alloying additions at the oxide-metal interface and/or sufficient thermionic electron conduction to permit

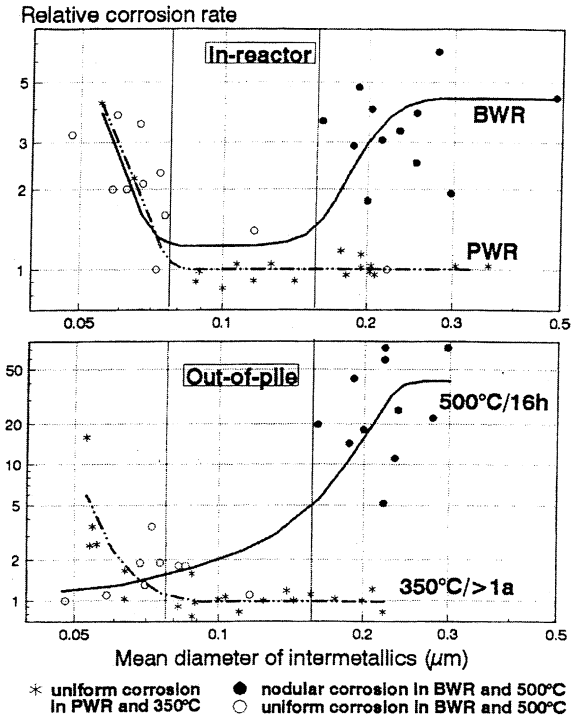

Fig. 36. Effect of second phase particle size on corrosion [146].

galvanic currents between the SPPs and the Zr matrix. The necessity for high pressure simultaneously with high temperature is not clear since the pressure dependence of oxidation under conditions not giving rise to nodular corrosion is very small [6]. The pressure below which nodular corrosion is not observed at 500 °C (Fig. 37) [147] is not correlated with any clear mechanistic effect but may again be related to the electronic conductivity of the oxide. Since the mechanistic conclusions reached from tests in $\geqslant$500 °C steam may not be applicable to nodular corrosion at much lower temperatures in BWR's, and most of the many mechanistic hypotheses [11] for nodule nucleation are based on the evidence from such high temperature/high pressure steam tests, attempts to try to reach conclusions about the mechanism will as far as possible, use in-reactor data.

It is necessary first to establish the important factors in corrosion, and especially the nodular corrosion process, in BWR's:

- *Radiation field*: There are many components of the radiation field in reactor, not all of which will be important in the phenomena observed.

(i) Fast neutron: such irradiation is necessary for the redistribution of the alloying elements in the SPPs into the metal matrix [113], and also possibly into the oxide matrix. The key factors in the oxide growth process are probably occurring at the oxide/metal interface, so that any redistribution that occurs in the oxide (especially after the SPPs have become oxidised) will probably be of only secondary importance (e.g. promoting cracking in the oxide). In any case nodules nucleate early in the life of the fuel cladding before much of this redistribution has occurred, and do not show a frequency distribution that follows the neutron flux profile. The effects of fast neutron redistribution of the intermetallic Fe persist when pre-irradiated specimens are repolished and corroded out-reactor [115], and can also explain the lack of any change in corrosion rate on changing from oxygenated to hydrogenated water chemistry in in-reactor loop tests [128], or changes from high to low flux position [129].

(ii) β-radiation: This will contribute to the production of radiolytic species in the water, and to enhanced electronic conductivity in the oxide [96], but displacement damage in either metal or oxide will be too small to make any significant contribution to fast neutron (and primary knock-on) effects [111]. Effects of dissimilar materials that are β-emitters will be negligible when compared with the background β-flux [126].

(iii) γ-radiation: This is the primary contributor to radiolytic species production [148], and will be an important contributor to enhanced oxide conductivity [149]. Displacement effects in zirconia from γ-radiation production of electron–positron pairs are negligible, since the energy (511keV) is too low to cause displacements in zirconia which requires nearly 1 MeV electrons. Compton electron production (which is only a scattering and not an absorption process), also gives too low an energy. Photoelectrons from absorption of $\sim$1 MeV gammas are energetic enough, but the yield is low for >1 MeV gammas.

- *Radiolytic species*: It was assumed from the start [148] that nodular corrosion phenomena were caused by the presence of the radiolytic species, since Zircaloys do not undergo such effects in oxygenated water in the laboratory. However, specific effects of any radiolytic radical species reaching an oxidised zirconium surface have never been demonstrated, and annihilation of such radicals at the zirconia surface would be expected to be rapid. While such species might affect the rates of reactions at the oxide/water interface, the oxidation rates of zirconium alloys are controlled within the oxide. Surface reaction rates have little or no effect on the corrosion rate, as is shown by the absence of any effect on the oxide growth rate in the pH range from $\sim$1 (H_2SO_4, HNO_3) to $\sim$14 (NH_4OH) excepting specific effects resulting from F^- or LiOH, NaOH and KOH.

One of the longer lived products of radiolysis (H_2O_2) has been argued to dissolve ZrO_2 films [106], perhaps

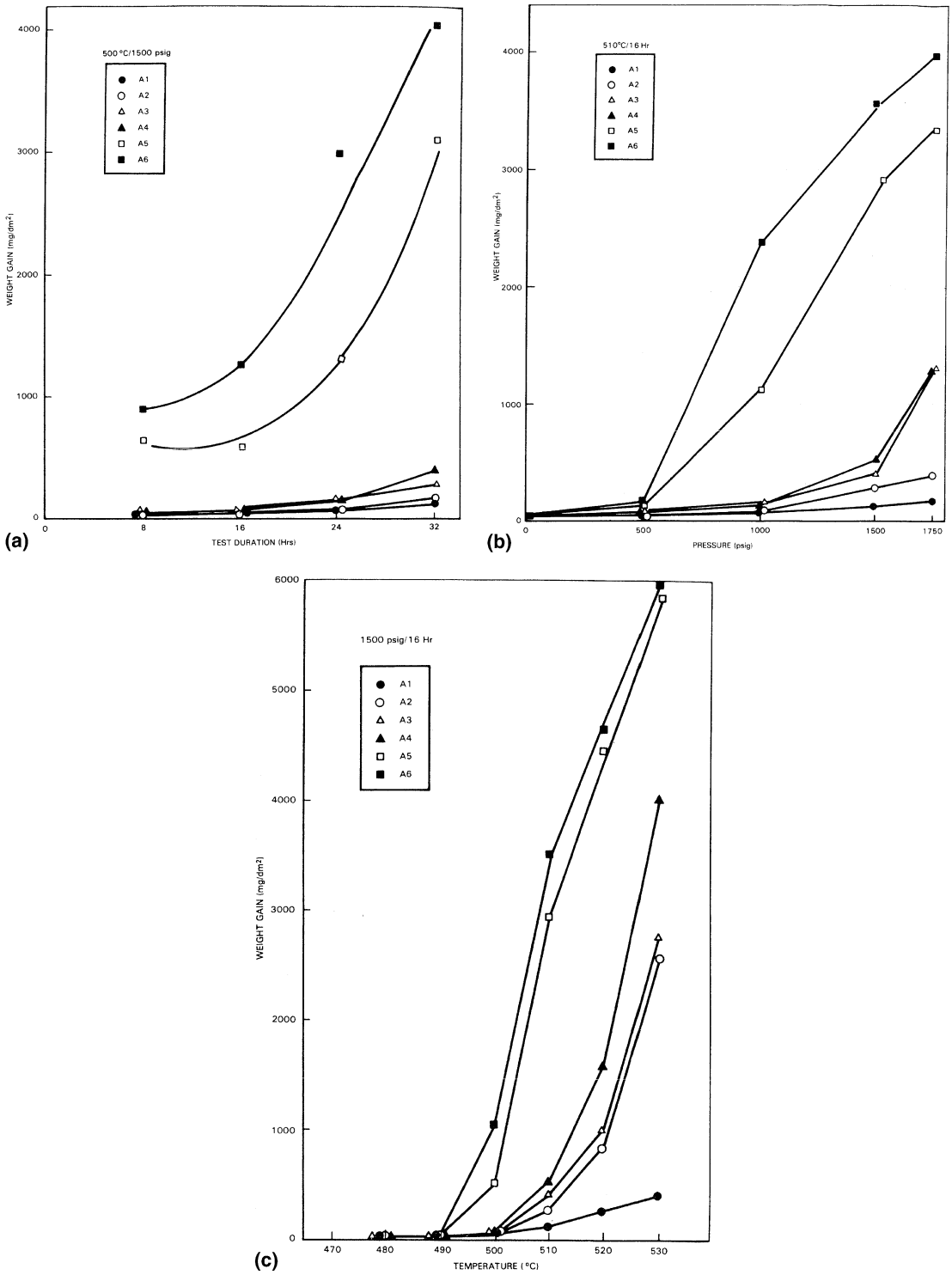

Fig. 37. (a) Weight gains of Zircaloy-2 samples as a function of test duration in 500 °C, 1500 psig (102 bars) steam [147]. (b) Weight gains of Zircaloy-2 cladding samples as a function of test temperature performed in 1500 psig (102 bars) steam for 16 h [147]. (c) Weight gains of Zircaloy-2 samples as a function of system pressure in 510 °C steam for 16 h [147].

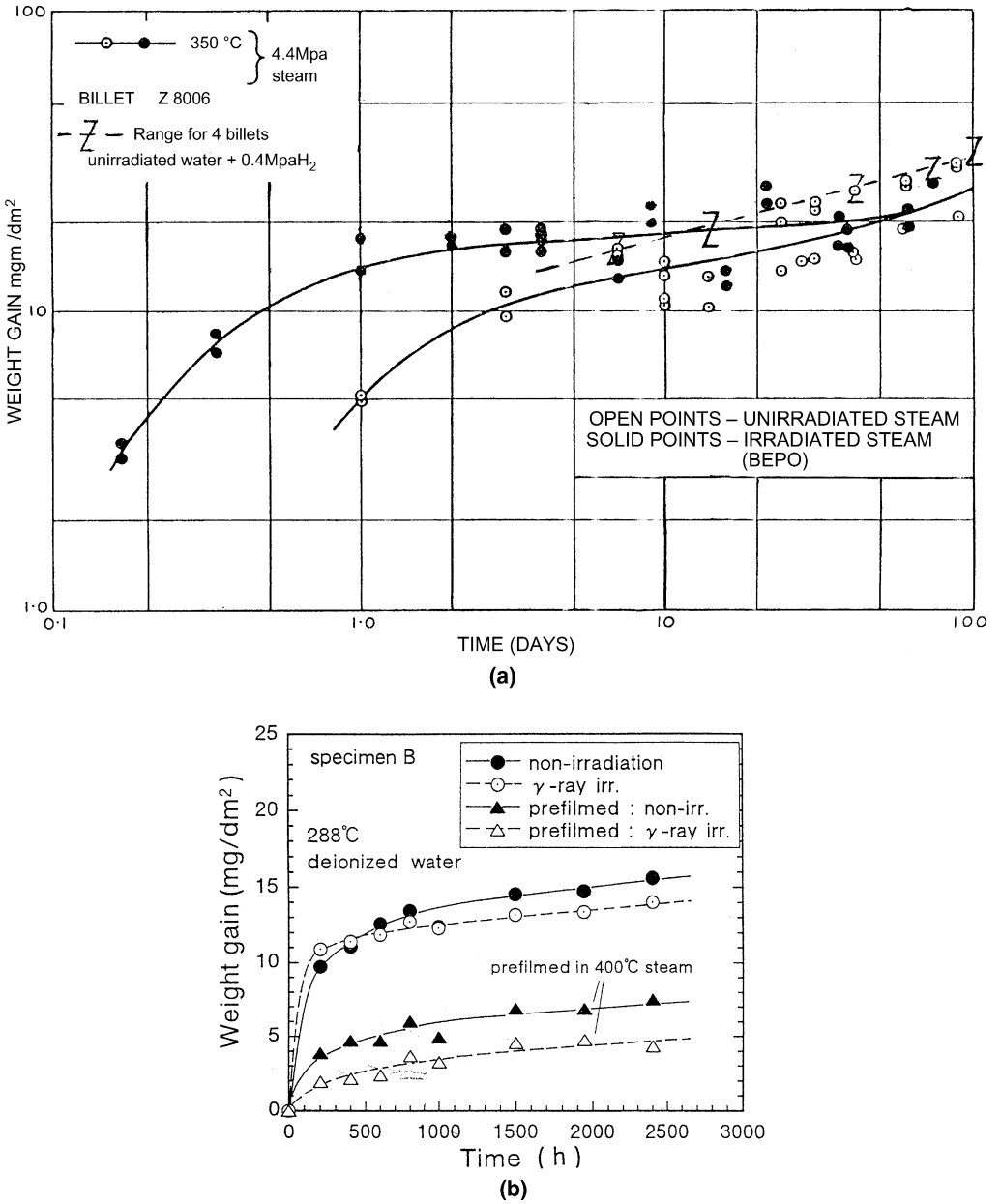

Fig. 38. (a) Oxidation of Zircaloy-2 in irradiated steam at 350 °C [150]. (b) Weight gains of specimen B in 288 °C pure water with and without γ-ray irradiation [107].

locally. Some supporting evidence for this has been obtained (Fig. 38) from specimens corroded in water under γ-irradiation [107,150] and this has been supported by measurements of the dissolution of bulk stabilised zirconia specimens under similar conditions [107]. This could certainly provide a contributory mechanism for the enhanced uniform corrosion in BWRs seen on cladding with too small an initial SPP size, but does not explain nodular corrosion nucleation since no localised corrosion was observed in these experiments. No localised effects were observed either during the enhanced growth of interference coloured oxides at 50 °C in ATR [100].

- *Galvanic effects*: It has been known from the early 'mixed grid' experiment [86] that a galvanic couple with either stainless steel or a nickel alloy in contact with or in close proximity to the Zircaloy cladding stimulated the initiation and growth of corrosion

nodules. This is the basic mechanism of the shadow corrosion discussed earlier. Similar effects accompanied the implantation of platinum plugs in Zircaloy or the bonding to a nickel alloy [128]. Isobe et al. [151] showed that welding a $10mm^2$ piece of a $Zr(Fe_{0.66}, Cr_{0.33})$ intermetallic on to a Zr–1.3% Sn precipitate free specimen with poor corrosion resistance in 633 K water protected the whole $1 \times 3 \times 0.1$ cm specimen from gross corrosion and oxide spalling in a 15 day test in 633 K water. Both the precipitate-free Zr–1.3%Sn alloy and the intermetallic alone showed poor corrosion resistance in a similar test (>650 mg/dm^2 with spalling for the former, unspecified for the latter). It appears that some galvanic protection has been occurring, but whether it was 'anodic protection' as postulated by the authors is not clear. In this instance both parts of the couple showed thin black oxide films, whereas the galvanic couples with Pt and Ni in Johnson's loop experiments [18] showed both enhanced corrosion of the Zircaloy in contact with the implants and enhanced shadow corrosion for non-contact Zircaloy specimens in close proximity to the implants.

There is no evidence for a size dependence of these effects so it is possible that in Zircaloys the intermetallic particles in the specimen surfaces are forming galvanic couples with the α-Zr matrix. Weidinger et al. [152] argued from electrochemical measurements that the intermetallic particles were the cathodes, however, their electrochemical measurements were not made in an oxygenated solution chemistry that would have been analogous to BWR chemistry. If the intermetallics are cathodic then the matrix surrounding them should be anodically polarised and hence the pre-transition corrosion rates should be increased over those of unalloyed zirconium. This is certainly the observation in the case of Zr alloys oxidised in oxygen [16] but cannot easily be tested in water because of the very irregular oxide growth and early spalling of the oxide on unalloyed Zr.

If this electrochemical couple is the basic mechanism of SPP effects, then the observation that large scale galvanic effects (e.g. shadow corrosion) are prominent only in BWR water chemistry, and are not evident in PWR chemistry (because all materials exhibit the reversible hydrogen potential in PWRs and so the electrochemical potentials driving these effects are small or zero), then we might expect micro-galvanic effects between SPPs and the matrix also to be more prominent in BWRs. In such a scenario, then, the size and distribution of the SPPs become clearly important for they define the ratio of cathode area to anode area. Larger diameter SPPs would be able to polarize (and enhance the corrosion) in a larger area of α-Zr surface around them, and obviously local clusters of SPPs would be even more effective. This would then explain the conclusion that nodule nucleation occurs at clusters of intermetallic particles [153]. The similarity between the cross-sectional shape of BWR nodules (Fig. 1 in Ref. [154]) and the areas of enhanced corrosion adjacent to a Ni alloy weld (Fig. 2.15c in Ref. [128]) is notable. The observation of nodules initiating primarily under stainless steel grids [86] then indicates that the additional polarisation generated by the stainless steel can tip the electrochemical balance between SPPs and the matrix of fuel cladding in close proximity so that nodules can initiate at sites producing insufficient galvanic current to initiate nodules in the absence of the grid. Unfortunately Weidinger et al. [151] did not extend their corrosion tests to demonstrate that the 'nodule precursors' that they observed actually became nodules after longer exposures. Very small SPPs that rapidly shrink during irradiation (or dissolve completely) would be unable to generate large enough galvanic currents to initiate nodules.

13. Water chemistry effects

If nodular corrosion is a micro-galvanic corrosion effect between the SPPs and the surrounding α-Zr matrix then the water chemistry becomes important for several reasons:

(i) Changing the redox potential of the coolant (e.g. by hydrogen additions) should eventually eliminate the galvanic potentials driving the effects. The evidence (Fig. 32) suggests [9,11] that this condition will not be reached until the hydrogen content of the water exceeds 10 cc/kg. Prior to this point it is not clear whether the rate of growth of nodules is proportional to (say) the oxygen concentration in the reactor water, or is relatively independent of this.

(ii) Impurities that enhance the water conductivity under irradiation should enhance the effect by increasing the return current in the SPP/α-Zr cell. This may have been one of the contributions of the copper in the water to the enhanced nodular corrosion in CILC failures [154]. Its concentration and deposition within cracks in the thick oxides on the severely corroded areas of cladding may then have been a consequence of the local conditions. The primary effect of Cu would have been the generation of a rigid crud layer that permitted cracking, steam blanketting and high temperatures to develop.

In practice, the major reduction in the incidence of severe nodular corrosion in BWRs has been achieved by a combination of careful control of the SPP size of the Zircaloy-2 (not too small and not too big), combined with improved control of the water chemistry. As a result of this, there has been little incentive recently to carry out further mechanistic studies in this area. The examples of enhanced spacer shadow corrosion have resulted in several studies confirming its largely galvanic

corrosion component [85,87,127], but the necessity of controlling the Fe chemistry in the coolant suggests that there is another significant factor, perhaps associated with the electrical properties of the crud deposits in contact with the ZrO_2 surface. Again the incentive to study such effects is absent since a satisfactory 'ad hoc' method of preventing such events in the future seems to have been identified.

14. Conclusions

Opinions about the mechanisms that are important in determining the corrosion rates of zirconium alloys have changed over the years. Some factors that were thought to be important during early studies have not revealed supporting evidence. Thus:

- There seems to be little or no supporting evidence for the idea that displacement damage from fast neutrons and the correspondingly increased diffusion rates in the protective oxide result in direct enhancement of the corrosion rates [9,11]. Evidence for such damage in oxides grown in-reactor has been minimal or non-existent. Fast neutron irradiation appears to affect the corrosion rate by redistributing alloying additions, such as Fe, from the second phase particles to a metastable solid solution in the zirconium matrix [115,122]. This process appears to be operating in both PWR and BWR chemistry, and explains instances where changing from oxygenated to hydrogenated water chemistry [128], or from high to low flux [129], had no effect on corrosion rates since such changes would not reverse the extent of the radiation induced redistribution of Fe.
- Although a monoclinic to tetragonal phase change in ZrO_2 during irradiation has been demonstrated in low temperature experiments where chemically stabilising elements were apparently absent, the t-ZrO_2 produced is metastable and reverts to m-ZrO_2 if exposed to ~300 °C water. This is in line with the extensive evidence for degradation of tetragonal zirconia ceramics by water or water vapour at temperatures as low as ~100 °C, and with the evidence that, if anything, irradiated ZrO_2 corrosion films contain less t-ZrO_2 than those produced in laboratory autoclaves. This would also provide a mechanism that could degrade the oxide film from the outside in.
- No evidence has been produced for any direct effect of radiolytic radical species on a rate controlling process at the surface of ZrO_2 corrosion films. However, it has been proposed that the high peroxide concentration in BWR water acts by dissolving the ZrO_2 locally [107] (or possibly by dissolving SnO_2 or Fe_2O_3 crystallites in the oxide grain boundaries). This hypothesis seems to be borne out by weight losses (or lower than expected weight gains) during corrosion of Zircaloy specimens and ZrO_2 ceramics during γ-irradiation in ~300 °C water [107]. The effect of radiolytic species on the redox potentials of the various metal phases present is probably the most important factor here.
- Enhanced corrosion in PWRs by the concentration of LiOH in thick porous oxides under heat flux, when the saturation temperature of the water is exceeded, is perhaps not possible except at the very end of a reactor cycle, when the boric acid concentration is close to zero. While the boric acid concentration remains above ~100 ppmB the LiOH concentration effect is negated if the boric acid is also concentrated by the same factor as the LiOH concentration. No evidence of Li/B fractionation by boiling has been found [138]; but it may be that boric acid does not concentrate to the same extent as LiOH in oxide films grown in-reactor, due to the large size of the borate ion [108], thus permitting accelerated corrosion.

Thus:

- The redistribution of alloying elements by fast neutron irradiation, especially Fe, is now seen as a primary contributor to enhanced corrosion in PWRs, where alloys with low (or no) Fe contents, and alloys where the Fe is locked up in second phase particles that are radiation resistant, show much less acceleration of in-reactor corrosion rates than any variant of Zircaloy-4. In BWRs the rapid redistribution of Fe from very small SPPs eliminates the regular nodular corrosion susceptibility in the alloys, but causes enhanced uniform corrosion. The late reappearance of nodular corrosion in such batches of cladding has yet to be satisfactorily explained.
- Large increases in the electronic conductivity of zirconia corrosion films produced by a combination of β^- and γ radiation increase the corrosion rates of Zircaloy in the thin film region, where electronic conduction through the oxide is the rate limiting process for oxide growth. It is not known to what extent this mechanism is operating in the thick film region, since we have no evidence for the potential difference across the oxide under these conditions. Electrochemical rest potentials in high temperature water are largely determined by the chemical reactions at the oxide/environment interface, which are not controlling the corrosion rate.
- Galvanic corrosion, resulting from the residual potential differences observed between metallic phases in BWR water chemistry, but not in the high hydrogen concentrations in PWR water, is a major factor in the regularly observed 'shadow corrosion' phenomena where dissimilar metals are in close proximity in BWRs. The increased conductivity of the

surface oxide films and the water during in-reactor exposures is the primary additional factor necessary for the occurrence of such effects. The separation distance over which shadow effects can be seen is determined by the enhanced conductivity in the overall system. Since shadow phenomena have been observed with dissimilar Zircaloys (i.e. no stainless steel or Ni alloy present), and Zr intermetallics have different electrochemical potentials from the Zr matrix, it should be considered whether or not nodular corrosion in BWRs is a micro-version of shadow corrosion. Such an hypothesis would provide a rationale for the dependence of nodular corrosion on the size and number density of the SPPs (too small a cathodic area would not supply a high enough galvanic current), and on the precise annealing temperature relative to the $\alpha/\alpha + \beta$ boundary in the alloy (compositional changes in the SPP would affect its electrochemical potential and hence the available potential difference with the surrounding matrix).

- Crevice corrosion effects must always be considered when the geometry warrants it, and undoubtably such effects can be present in solutions (e.g. LiOH) where concentration in a tight crevice is possible even in the absence of heat transfer. However the 5mm gaps over which shadow corrosion effects have been seen are clearly too big for any crevice concentration effects to be present. In a situation such as the end-fitting crevice between a Zr–2.5Nb pressure tube and its 410 stainless steel end fitting the fraction of enhanced oxide growth on the Zr–Nb tube resulting from the concentration of LiOH in the crevice and from the galvanic cell set up by the stainless steel is difficult to judge. However a fraction of the cathodic component of the Zr/Nb corrosion reaction (hydrogen absorption reaction) has certainly been transferred to the stainless steel so both mechanisms may be operating.

There are obviously a number of circumstances where additional information is necessary in order to distinguish which of several possibilities is the actual operating mechanism, or which combination of the various possible mechanisms is functioning. It is hoped that the arguments presented here will stimulate further experiments to resolve these questions.

References

[1] H.G. Rickover, L.D. Geiger, B. Lustman, History of the development of zirconium alloys for use in nuclear reactors, US Report, Division of Naval Reactors, Washington, DC, TID-26740, March 1975.

[2] D.E. Thomas, in: B. Lustman, F. Kerze (Eds.), Metallurgy of Zirconium, Vol. VIII-4, McGraw-Hill, National Nuclear Energy Series, New York, 1955 (Chapter 11, Pt. II).

[3] A.S. Zaimovskii, A.V. Nikulina, I.G. Rezhetnikov, Zirconium Alloys for Nuclear Energy, Energoatomizdat, Moscow, 1994 (in Russian).

[4] S. Kass, in: Proceedings of the Symposium on the Corrosion of Zirconium Alloys, New York, ASTM-STP-368, American Soc. for Testing and Materials, Philadelphia, PA, 1963, p. 3040.

[5] B. Cox, J. Nucl. Mater. 28 (1968) 1.

[6] B. Cox, in: M.G. Fontana, R.W. Staehle (Eds.), Advances in Corrosion Science and Technology, Vol. 5, Plenum, NY, 1976, p. 173.

[7] B. Wadman, Mechanics of Uniform Corrosion of Zirconium Alloys in Water and Steam, Phd thesis, Chalmers Univ., Göteborg, Sweden, 1993.

[8] D. Lim, N.A. Graham, D.O. Northwood, The degradation of zirconium alloys in nuclear reactors – a review, Canadian Report, Atomic Energy Control Board, Ottawa (Now Canadian Nuclear Safety Commission) INFO-0174, January 1986.

[9] Corrosion of zirconium alloys in nuclear power plants, International Atomic Energy Agency, Vienna, Austria, TECDOC-684, January 1993.

[10] C. Lemaignan, A.T. Motta, Zirconium Alloys in Nuclear Applications, Materials Science and Technology, Nuclear Materials Pt. 2, VCH Verlagsgesellschaft mbH, Weinheim, Ger. 10B, 1995.

[11] Waterside corrosion of zirconium alloys in nuclear power plants, International Atomic Energy Agency, Vienna, Austria, TECDOC-996, 1998.

[12] H. Bailly, D. Ménessier, C. Prunier (Eds.), The Nuclear Fuel of Pressurized Water Reactors and Fast Reactors: Design and Behaviour, Collection du Commissariat á L'Énergie Atomique, English Edition, Intercept, Andover, Hants, UK, 1999.

[13] R.A. Ploc, J. Nucl. Mater. 28 (1968) 48.

[14] J.N. Wanklyn, in: Proceedings of the Symposium on the Corrosion of Zirconium Alloys, New York, ASTM-STP-368, American Soc. for Testing and Materials, Nov. 1963, p. 58.

[15] B. Cox, J. Aust. Inst. Metals 14 (1969) 123.

[16] R.D. Misch, C. van Drunen, in: Proceedings of the USAEC Symposium on Zirconium Alloy Development, Castlewood, CA, US Report GEAP-4089, Vol. II, November 1962, Paper 15.

[17] B. Cox, The Effects of Some Alloying Additions on the Oxidation of Zirconium in Steam, UK Report, AERE-R4458, UK Atomic Energy Authority, Harwell, 1963.

[18] B. Cox, J. Electrochem. Soc. 108 (1961) 24.

[19] J.N. Wanklyn, C.F. Britton, D.R. Silvester, N.J.M. Wilkins, J. Electrochem. Soc. 110 (1963) 856;
J.N. Wanklyn, C.F. Britton, D.R. Silvester, N.J.M. Wilkins, J. Nucl. Mater. 5 (1962) 326.

[20] D. Charquet, R. Hahn, E. Ortlieb, J.-P. Gros, J.-F. Wadier, in: L.F.P. van Swam, C.M. Eucken (Eds.), Proceedings of 8th International Symposium on Zr in the Nuclear Industry, San Diego, CA, ASTM-STP-1023, American Society for Testing and Materials, Philadelphia, PA, USA, 1989, p. 405.

[21] R.S. Ambartsumyan, A.A. Kisilev, R.V. Grebenikov, V.A. Myshkin, L.J. Tsuprun, A.V. Nikulina, in: Proceedings of 2nd International Conference on the Peaceful Uses of Atomic Energy, Vol. 6, Geneva, CH, United Nations, NY, 1958, p. 12.
[22] V.A. Tsykanov, E.F. Davidov, B.F. Samsonov, V.K. Zhamardin, A.B. Andreeva, V.S. Belokopikov, A.G. Finiko, G.I. Maerzhina, A.V. Nikulina, V.Th. Tonkoy, M.B. Fiventskii, A.S. Sotnikov, in: Proceedings of the 1st International Conference on Reactor Materials Behaviour, Vol. 6, Alushta '78, Atominform, Moscow, 1978, p. 261.
[23] B. Cox, J.P. Pemsler, J. Nucl. Mater. 28 (1968) 73.
[24] J.L. Whitten, J. Electrochem. Soc. 115 (1968) 58.
[25] U. Brossmann, R. Würscheim, U. Södervall, H.E. Schaefer, J. Appl. Phys. 85 (1999) 7646.
[26] N. Ramasubramanian, J. Nucl. Mater. 55 (1975) 134.
[27] X. Guo, R.-Z. Yuan, Solid State Ion. 80 (1995) 159.
[28] X. Guo, J. Mair, J. Electrochem. Soc. 148 (2001) E121.
[29] M. Oskarsson, E. Ahlberg, K. Pettersson, J. Nucl. Mater. 295 (2001) 97.
[30] M. Oskarsson, E. Ahlberg, U. Andersson, K. Pettersson, J. Nucl. Mater. 297 (2001) 77.
[31] G. Nagy, Z. Kerner, G. Battistig, A. Pinter-Csordas, J. Balogh, T. Pajkossy, J. Nucl. Mater. 297 (2001) 62.
[32] B. Cox, Y.-M. Wong, T. Huang, J. Nucl. Mater. 223 (1995) 209.
[33] A.L. Bacarella, A.L. Sutton, J. Electrochem. Soc. 112 (1965) 546.
[34] M.L. Brown, G.N. Walton, J. Nucl. Mater. 66 (1977) 44.
[35] B. Cox, J. Nucl. Mater. 31 (1969) 48.
[36] P.J. Shirvington, J. Nucl. Mater. 37 (1970) 177.
[37] K. Hauffe, Oxidation of Metals, Plenum, N.Y., 1965.
[38] D.H. Bradhurst, J.E. Draley, C.J. vanDrunen, J. Electrochem Soc. 112 (1965) 1171.
[39] S.B. Dalgaard, Transference Numbers and Their Relation to In-Reactor Oxidation of Zirconium, Canadian Report, AECL-2066 Atomic Energy of Canada, Chalk River, ON, 1964.
[40] A. Fiegna, P. Weisgerber, J. Electrochem. Soc. 115 (1968) 369.
[41] W. Hübner, B. Cox, Electrochemical Properties and Oxidation of some Zirconium Alloys in Molten Salt at 300–500 °C, Canadian Report, AECL-4431, Atomic Energy of Canada, Chalk River, ON, 1973.
[42] N. Ramasubramanian, J. Electrochem. Soc. 116 (1969) 1237.
[43] B. Cox, C. Roy, Electrochem. Tech. 4 (1966) 121.
[44] R.A. Ploc, The Interpretation of a Transmission Electron Diffraction Pattern from Thin ($\leqslant$2000 Å) ZrO_2 Films, Canadian Report, AECL-2794, Atomic Energy of Canada, Chalk River, ON, 1967.
[45] R.A. Ploc, J. Nucl. Mater. 110 (1982) 59.
[46] R.A. Ploc, J. Nucl. Mater. 113 (1983) 75.
[47] R.A. Ploc, J. Nucl. Mater. 115 (1983) 110.
[48] G. David, R. Geschier, C. Roy, J. Nucl. Mater. 38 (1971) 329, 344.
[49] A.T. Donaldson, H.E. Evans, Oxidation-induced Creep in Zircaloy-2, Pts I–III, UK Reports, RD/T/N4855, 4952 and 4976, Central Electricity Generating Board, Berkeley Nuclear Labs, Berkeley, UK, 1980.
[50] E. Hillner, D.G. Franklin, J.D. Smee, J. Nucl. Mater. 278 (2000) 334, and Refs. therein.
[51] B. Cox, J. Less. Comm. Metals 5 (1963) 325.
[52] V. Urbanic, M. Griffiths, in: G.P. Sabol, G.D. Moan (Eds.), Proceedings of 12th International Symposium on Zr in the Nuclear Industry, Toronto, ON, Canada, ASTM-STP-1354, American Soc. for Testing and Mater., W. Conshohocken, PA, 2000, p. 641.
[53] K. Takeda, H. Anada, in: G.P. Sabol, G.D. Moan (Eds.), Proceedings of 12th International Symposium on Zr in the Nuclear Industry, Toronto, ON, Canada, ASTM-STP-1354, p. 592; K. Takeda, H. Anada, in: 11th International Symposium on Zr in the Nuclear Industry, Baltimore, MD, USA, ASTM-STP-1295. American Soc. For Testing and Mater. W. Conshohocken, PA, 1996, p. 35.
[54] H.-J. Beie, A. Mitwalsky, F. Garzarolli, H. Ruhmann, H.-J. Sell, in: A.M. Garde, E.R. Bradley (Eds.), Proceedings of 10th International Symposium on Zr in the Nuclear Industry, Baltimore, MD, USA, ASTM-STP-1245, American Soc. for Testing and Mater., Philadelphia, PA, 1994, p. 615.
[55] B. Wadman, Z. Lai, H.-O. Andrén, A.-L. Nyström, P. Rudling, H. Pettersson, in: A.M. Garde, E.R. Bradley (Eds.), Proceedings of 10th International Symposium on Zr in the Nuclear Industry, Baltimore, MD, USA, ASTM-STP-1245, p. 579.
[56] R.A. Ploc, S.B. Newcomb, in: Proceedings of 3rd International Conference on Microscopy of Oxidation, Trinity Hall, Cambridge, UK, Inst. of Materials, London September 1996, p. 475.
[57] B. Cox, J. Nucl. Mater. 41 (1971) 96.
[58] J. Godlewski, P. Bouvier, G. Lucazeau, L. Fayette, in: G.P. Sabol, G.D. Moan (Eds.), Proceedings of 12th International Symposium on Zr in the Nuclear Industry, Toronto, ON, Canada, ASTM-STP-1354, American Soc. for Testing and Mater., W. Conshohocken, PA, USA, 2000, p. 877 (and Refs. therein).
[59] Papers on ZrO_2 phase transformations in Section 1, in: Proceedings of 2nd International Conference on the Sci. and Tech. of Zirconia (Zirconia '83), Stuttgart, Germany, Adv. in Ceramics, Vol. 12, Amer. Ceram. Soc., Columbus, OH, USA, 1983, p. 1.
[60] Y. Ishii, J.M. Sykes, in: Proceedings of 4th International Conference on Microscopy of Oxidation, Trinity Hall, Cambridge, UK, Science Reviews, 2000, Inst. of Physics, London, 1999, p. 23.
[61] M.A. Maguire, in: Proceedings of 9th International Symposium on the Environmental Degradation of Materials in Nuclear Power Systems, Newport Beach, CA, USA, 1999.
[62] B. Cox, J. Nucl. Mater. 27 (1968) 1.
[63] X. Guo, J. Mater. Sci. 36 (2001) 3737, and Refs. therein.
[64] M. Hirano, Brit. Ceram. Trans. J. 91 (1992) 139, and Refs. therein.
[65] M. Yoshimura, Ceram. Bull. 67 (1988) 1950, and Refs. therein.
[66] J. Godlewski, in: A.M. Garde, E.R. Bradley (Eds.), Proceedings of 10th International symposium on Zr in the Nuclear Industry, Baltimore, MD, USA, ASTM-STP-1245, American Society for Testing and Mater., Philadelphia, PA, USA, 1994, p. 663.

[67] H. Coriou, L. Grall, J. Meunier, M. Pelras, H. Willermoz, J. Nucl. Mater. 3 (1962) 320.
[68] M. Oskarsson, E. Ahlberg, K. Pettersson, J. Nucl. Mater. 295 (2001) 126.
[69] B. Cox, M. Ungurelu, Y.-M. Wong, C. Wu, in: E.R. Bradley, G.P. Sabol (Eds.), Proceedings of 11th International Symposium on Zr in the Nuclear Industry, Garmisch-Partenkirchen, Germany, ASTM-STP-1295, American Society for Testing and Mater., W. Conshohocken, PA, USA, 1996, p. 114.
[70] D.T. Foord, S.B. Newcomb, in: Proceedings of 3rd International Conference on Microscopy of Oxidation, Trinity Hall, Cambridge, UK, Inst. of Materials, London, 1996, p. 488.
[71] B. Cox, H.I. Sheikh, J. Nucl. Mater. 249 (1997) 17.
[72] B. deGélas, G. Béranger, P. Lacombe, J. Nucl. Mater. 28 (1968) 185.
[73] B. Cox, T. Johnston, Corrosion 18 (1962) 33t.
[74] A.M. Garde, G.P. Smith, R.C. Pirek, in: E.R. Bradley, G.P. Sabol (Eds.), Proceedings of 11th International Symposium on Zr in the Nucl. Industry, Garmisch-Partenkirchen, Germany, ASTM-STP-1295 (see Table 6), American Society for Testing and Mater., W. Conshohocken, PA, USA, 1996, p. 407.
[75] T. Kido, in: R.E. Gold, E.P. Simmons (Eds.), Proceedings of 6th International Symposium on Environmental Degradation of Materials in Nuclear Power Systems – Water Reactors, San Diego, CA, USA, American Society for Testing and Materials, Philadelphia, PA, USA, 1988, p. 449.
[76] M. Blat, L. Legras, D. Noel, H. Amanrich, in: G.P. Sabol, G.D. Moan (Eds.), Proceedings of 12th International Symposium on Zr in the Nuclear Industry, Toronto, ON, Canada, ASTM-STP-1354, American Soc. for Testing and Mater., W. Conshohocken, PA, USA, 2000, p. 563.
[77] A. van der Linde, A.C. Letsch, E.M. Hornsveld, Some Observations on Pitting Corrosion in the Zircaloy Cladding of Fuel Pins Irradiated in a PWR Loop, Netherlands Report, ECN-51 Netherlands Energy Research Foundation, Petten Nov. 1978.
[78] F.H. Krenz, A Preliminary Study of the Effects of Added Fluoride on the Corrosion of Zr-2 in Water at 300 °C, Canadian Report, AECL-1507, Atomic Energy of Canada, Chalk River, ON, March 1962.
[79] L.F.P. van Swam, S.H. Shann, in: C.M. Eucken, A.M. Garde (Eds.), Proceedings of 9th International Symposium on Zr in the Nuclear Industry, Kobe, Jp, ASTM-STP-1132, American Soc. for Testing and Mater., Philadelphia, PA, USA, 1991, p. 758.
[80] H. Stehle, W. Kaden, R. Manzel, Nucl. Eng. Des. 33 (1975) 155.
[81] F.W. Trowse, R. Sumerling, A. Garlick, in: A.L. Lowe Jr., G.W. Parry (Eds.), Proceedings of 3rd International Conference on Zr in the Nuclear Industry, Québec City, PQ, Canada, ASTM-STP-633, American Society for Testing and Mater., Philadelphia, PA, USA, 1977, p. 236.
[82] W. Goll, I. Rey, in: Proceedings of 13th International Symposium on Zr. in the Nucl. Industry, Annecy, Fr, ASTM-STP-1423, American Society for Testing and Mater., W. Conshohocken, PA, USA, 2001, p. 80.
[83] J.-S.F. Chen, R.B. Adamson, in: Proceedings of International Topical Meeting on LWR Fuel Performance, W. Palm Beach, FL, American Nuclear Soc., La Grange Pk, IL, USA, 1994, p. 309.
[84] B. Cox, R. Beauregard, D.R. O'Boyle, Corrosion Observations of Two Zircaloy-4 Fuel Channels and the Associated Fuel Cladding, US Report EPRI-NP-6515, Appendix D, Electric Power Research Institute, Palo Alto, CA, 1989.
[85] H.-U. Zwicky, H. Loner, B. Andersson, C.-G. Wiktor, J. Harbottle, in: Proceedings of International Topical Meeting on LWR Fuel Performance, Vol. 1, Park City UT, American Nuclear Soc. La Grange Pk, IL, USA, 2000, p. 459.
[86] R. Sumerling, A. Garlick, A. Stuttard, J.M. Hartog, F.W. Trowse, P. Sims, in: J.H. Schemel, T.P. Papazoglou (Eds.), Proceedings of 4th International Conference on Zr in the Nuclear Industry, Stratford-upon-Avon, UK, ASTM-STP-681, American Society for Testing and Mater., Philadelphia, PA, 1979, p. 107.
[87] A. Chatelain, B. Andersson, R.-G. Ballinger, G. Wikmark, in: Proceedings of International Topical Meeting on LWR Fuel Performance, Vol. 1, Park City UT, American Nuclear Soc. La Grange Pk, IL, USA, 2000, p. 485.
[88] B. Cox, K. Alcock, F.W. Derrick, J. Electrochem. Soc. 108 (1961) 129.
[89] V. Fidleris, J. Nucl. Mater. 159 (1988) 22.
[90] X. Iltis, F. Lefebvre, C. Lemaignan, in: E.R. Bradley, G.P. Sabol (Eds.), Proceedings of 11th International Symposium on Zr in the Nuclear Industry, Garmisch-Partenkirchen, Germany, ASTM-STP-1295, American Society for Testing and Mater., W. Conshohocken, PA, USA, 1996, p. 242.
[91] J.A. Spitznagel, L.R. Fleischer, W.J. Choyke, in: Proceedings of International Conference on Applications of Ion Beams to Metals, Albuquerque, NM, 1973, p. 87.
[92] N. Sasajima, T. Matsui, K. Hojou, S. Furano, H. Otsu, K. Izui, T. Muromura, Nucl. Instr. Methods Phys. Res. B 141 (1998) 487.
[93] O.T. Woo, G.M. McDougall, R.M. Hutchinson, V.F. Urbanic, M.Griffiths, C.E. Coleman, in: G.P. Sabol, G.D. Moan (Eds.), Proceedings of 12th International Symposium on Zr in the Nuclear Industry, Toronto, ON, Canada, ASTM-STP-1354, American Soc. for Testing and Mater., W. Conshohocken, PA, 2000, p. 709.
[94] L.W. Hobbs, F.W. Clinard Jr., S.J. Zinkle, R.C. Ewing, J. Nucl. Mater. 216 (1994) 291.
[95] F.W. Clinard Jr., D.L. Rohr, W.A. Ranken, J. Amer. Ceram. Soc. 60 (1977) 287.
[96] M.M.R. Howlader, C. Kinoshita, K. Shiiyama, M. Kutsuwada, M. Inagaki, J. Nucl. Mater. 265 (1999) 100.
[97] P.J. Harrop, N.J.M. Wilkins, J.N. Wanklyn, J. Nucl. Mater. 16 (1965) 290.
[98] W.J.S. Yang, R.P. Tucker, B. Cheng, R.B. Adamson, J. Nucl. Mater. 138 (1986) 185.
[99] G.J. Jenks, J.E. Baker, M.D. Silverman, Chemical Aspects of Corrosion of Zircaloy-2, US Report, ORNL-3262, Chapter 9, Oak Ridge Nat. Lab., Chemistry Div. Annual Rep. to 31/01/1962, p. 80.

[100] B. Cox, V. Fidleris, in: L.F.P. van Swam, C.M. Eucken (Eds.), Proceedings of 8th International Symposium on Zr in the Nuclear Industry, San Diego, CA, ASTM-STP-1023, American Society for Testing and Materials, Philadelphia, PA, USA, 1989, p. 245.
[101] S. Somiya, Hydrothermal Reactions for Materials Science and Engineering, Elsevier, London and New York, 1989.
[102] C.F. Britten, J.V. Arthurs, J.N. Wanklyn, J. Nucl. Mater. 15 (1965) 263.
[103] O.T. Woo, Y-P. Lin, D. Khatamian, in: Proceedings of 5th International Conference on Microscopy in Oxidation, Limerick, Eire, Aug. 2002, Sci. Revs. Materials at High Temperatures, Vol. 20 (2003) 593.
[104] X. Iltis, F. Lefebvre, C. Lemaignan, J. Nucl. Mater. 224 (1995) 109.
[105] X. Iltis, J. Nucl. Mater. 224 (1995) 121.
[106] V.G. Kritsky, N.G. Petrik, I.G. Berezina, V.V. Doilnitsina, in: Proceedings of IAEA Tech. Comm. Meeting, Řež, Czech Rep., October 1993, IAEA-TECDOC-927, p. 23.
[107] Y. Nishino, M. Endo, E. Ibe, T. Yasuda, J. Nucl. Mater. 248 (1997) 292.
[108] N. Ramasubramanian, P. Billot, S. Yagnik, in: Proceedings of 13th International Symposium on Zr in the Nuclear Industry, Annecy, Fr, ASTM-STP-1423, American Soc. for Testing and Materials, W. Conshohocken, PA, USA, 2001, p. 222.
[109] J.R. Johnson, Trans. AIME 212 (1958) 13.
[110] D. Simeone, J.L. Bechade, D. Gosset, A. Chevarier, P. Daniel, H.P. Pilliaire, G. Baldinozzi, J. Nucl. Mater. 281 (2000) 171.
[111] D. Simeone, D. Gosset, J.L. Bechade, A. Chevarier, J. Nucl. Mater. 300 (2002) 27.
[112] H.R. Peters, J.L. Harlow, in: E.R. Bradley, G.P. Sabol (Eds.), Proceedings of 11th International Symposium on Zr in the Nucl. Industry, Garmisch-Partenkirchen, Germany, ASTM-STP-1295, American Society for Testing and Mater., W. Conshohocken, PA, USA, 1996, p. 295.
[113] A.T. Motta, F. Lefebvre, C. Lemaignan, in: C.M. Eucken, A.M. Garde (Eds.), Proceedings of 9th International Symposium on Zr in the Nuclear Industry, Kobe, Jp, ASTM-STP-1132, American Soc. for Testing and Mater., Philadelphia, PA, USA, 1991, p. 718.
[114] M. Griffiths, R.W. Gilbert, G.J.C. Carpenter, J. Nucl. Mater. 150 (1987) 53.
[115] B.-C. Cheng, R.M. Kruger, R.B. Adamson, in: A.M. Garde, E.R. Bradley (Eds.), Proceedings of 10th International Symposium on Zr in the Nuclear Industry, Baltimore MD, USA, ASTM-STP-1245, American Society for Testing and Mater., Philadelphia, PA, USA, 1994, p. 400.
[116] W.K. Alexander, Hydriding of Hanford Production Reactor Zircaloy Process Tubes, Paper Presented at American Nuclear Soc. Conf. on Reactor Operating Experience, Atlantic City, NJ, July, 1967, and Report DUN-SA-34, 1967.
[117] W.K. Winegardner, B. Griggs, Zirconium Hydride Formation in Hanford Production Reactor Process Tubes, US Report, BNWL-588, Battelle North-West Laboratory, Richland, WA, December, 1967.
[118] R.L. Dillon, B. Griggs, Battelle North-West Laboratories, Quarterly Progress Report, July–September, 1965, Metallurgy Research Section, BNWL-166, 1966.
[119] B. Cox, J. Nucl. Mater. 175 (1990) 244.
[120] A.W. Urquhart, D.A. Vermilyea, W.A. Rocco, J. Electrochem. Soc. 125 (1978) 199.
[121] L. Lunde, J. Nucl. Eng. Des. 33 (1975) 178.
[122] S. Abolhassani, D. Gavillet, F. Groeschel, P. Jourdain, H.U. Zwicky, Recent Observations on the Evolution of the Secondary Phase Particles in Zircaloy-2 under Irradiation in a BWR up to High Burn-up, Proceedings of International Topical Meeting on LWR Fuel Performance, Vol. 1, Park City UT, American Nuclear Soc. La Grange Pk, IL, USA, 2000, p. 470.
[123] B. Andersson, The Enhanced Spacer Shadow Corrosion Phenomenon, Proceedings of Conf. on Verification of Fuel Element Performance, Kernforschungszentrum, Karlsruhe, February/March 2000, paper 9.
[124] B. Rossborg, A. Molander, in: Proceedings of IAEA Tech. Comm. Meeting, Rez, Czech Rep., IAEA-TECDOC-927, October 1993, pp 331.
[125] C. Lemaignan, J. Nucl. Mater. 187 (1992) 122.
[126] K. Lundgren, Radiation Induced Zircaloy Corrosion – Review of Actual Irradiation conditions in a BWR, Swedish Engineering Report, ABB Atom, September 1997.
[127] B. Andersson, M. Limback, G. Wikmark, E. Hauso, T. Johnsen, R.G. Ballinger, A.-C. Nystrand, in: Proceedings of 13th International Symposium on Zr. in the Nuclear Industry, Annecy, Fr, ASTM-STP-1423, American Society for Testing and Mater., W. Conshohocken, PA, USA, and Poster Presentation, On the Shadow Corrosion Mechanism, Same Conference 2001, p. 583.
[128] A.B. Johnson Jr., Zirconium Alloy Oxidation and Hydriding under Irradiation: Review of Pacific Northwest Laboratories' Test Program Results, US Report, EPRI-NP-5132, Electric Power Research Inst., PaloAlto, CA, April 1987.
[129] E. Hillner, D.G. Franklin, J.D. Smee, The Corrosion of Zircaloy-Clad Fuel Assemblies in a Geologic Repository Environment, Bettis Atomic Power Lab., W. Mifflin, Report WAPD-T3173, 1994.
[130] V.F. Urbanic, G.M. McDougall, A.J. White, A.A. Bahurmuz, Deuterium Ingress at Rolled Joints in CANDU Reactors, Paper presented at International Conference on Expanded and Rolled Joint Technology, Toronto, ON, Canada, Sept 1993; and Atomic Energy of Canada, Report RC-1116, November 1993.
[131] K.-Å. Magnusson, B. Andersson, R. Lundmark, in: Proceedings of TOPFUEL, Stockholm, SE, Paper #P2-26, European Nuclear Soc, 2001.
[132] R.S. Kaiser, R.-S. Miller, J.E. Moon, N.A. Pisano, in: Proceedings of ANS Topical Meeting on LWR Fuel Performance, Williamsburg, VA, American Nuclear Soc., La Grange Pk, Ill, 1988, p. 119.
[133] F. Garzarolli, W. Beck, H.P. Fuchs, E. Steinberg, R.A. Perkins, in: Proceedings of EPRI-Utility Workshop on Fuel Corrosion, Washington, DC, USA, Electric Power Res. Inst., Palo Alto, CA, July 1993.
[134] I.L. Bramwell, P.D. Parsons, D.R. Tice, in: C.M. Eucken, A.M. Garde (Eds.), Proceedings of 9th International

Symposium on Zr in the Nuclear Industry, Kobe, Jp, ASTM-STP-1132, American Society for Testing and Mater., Philadelphia, PA, 1991, p. 628.
[135] F. Garzarolli, W. Jung, H. Schoenfeld, A.M. Garde, G.W. Parry, P.G. Smerd, Waterside Corrosion of Zircaloy Fuel Rods, US Report, EPRI-NP-2789, Electric Power Research Inst., Palo Alto, CA, December 1982.
[136] F. Garzarolli, T. Broy, R.A. Busch, in: E.R. Bradley, G.P. Sabol (Eds.), Proceedings of 11th International Symposium on Zr in the Nuclear Industry, Garmisch-Partenkirchen, Germany, ASTM-STP-1295, American Soc. for Testing and Mater., W. Conshohocken, PA, USA, 1996, p. 850.
[137] P. Barberis, E. Ahlberg, N. Simic, D. Charquet, C, Lemaignan, G. Wikmark, M. Dahlbäck, M. Limbäck, P. Tägström, B. Lehtinen, in: Proceedings of 13th International Symposium on Zr in the Nuclear Industry, Annecy, France, ASTM-STP-1423, American Soc. for Testing and Mater., W. Conshohocken, PA, USA, 2001, p. 33.
[138] P. Billot, S. Yagnik, N. Ramasubramanian, J. Reybernes, D. Pêcheur, in: Proceedings of 13th International Symposium on Zr in the Nuclear Industry, Annecy, France, ASTM-STP-1423, p. 169.
[139] J.P. Mardon, A. Frichet, D. Charquet, J. Sevenat, P. Billot, T. Forgeron, in: Proceedings of TOPFUEL '99 Conference, Avignon, France, European Nuclear Society, 1999, p. 407.
[140] V.N. Shishov, M.M. Peregud, A.V. Nikulina, P.V. Shebaldov, A.V. Tselischev, A.E. Novoselov, G.P. Kobylyansky, Z.E. Ostrovsky, V.K. Shamardin, in: Proceedings of 13th International Symposium on Zr in the Nuclear Industry, Annecy, France, ASTM-STP-1423, American Soc. for Testing and Mater., W. Conshohocken, PA, USA, 2001, p. 758.
[141] A. Siebold, F. Garzarolli, in: Proceedings of 13th International Symposium on Zr in the Nuclear Industry, Annecy, France, ASTM-STP-1423, American Soc. for Testing and Mater., W. Conshohocken, PA, USA, 2001, p. 743.
[142] K. Govertsen, in: D. Smith (Ed.), Proceedings of 31st International Utility Nuclear Fuel Performance Conference, New Orleans, LA, USA, Entergy Operations Inc., August 2001.
[143] B. Cheng, EPRI Fuel Reliability Program Highlights, Palo Verde U2C9 Fuel Failures, Paper 3.
[144] M. Lippens, D. Haas, P. Gubel, J. van de Velde, C. van Loon, in: Proceedings of IAEA Specialist Meeting on the Influence of Power Reactors Water Chemistry on Fuel Cladding Reliability, San Miniato, Pisa, Italy, October 1981.
[145] B. Cox, J. Nucl. Mater. 249 (1997) 87.
[146] F. Garzarolli, R. Schumann, E. Steinberg, in: A.M. Garde, E.R. Bradley (Eds.), Proceedings of 10th International Symposium on Zr in the Nuclear Industry, Baltimore, MD, ASTM-STP-1245, American Soc. for Testing and Mater., Philadelphia, PA, USA, 1994, p. 709.
[147] B. Cheng, H.A. Levin, R.B. Adamson, M.O. Marlowe, V.L. Monroe, in: R.B. Adamson, L.F.P. van Swam (Eds.), Proceedings of 7th International Symposium on Zr in the Nuclear Industry, Strasbourg, France, ASTM-STP-939, American Soc. for Testing and Mater., Philadelphia, PA, USA, 1987, p. 257.
[148] W.G. Burns, P.B. Moore, A Survey of In-reactor Zirconium Alloy Corrosion, UK Report, AERE-R8184, United Kingdom Atomic Energy Authority, Harwell, March 1976, and Proceedings of BNES Conference on Water Chemistry of Nuclear Reactor Systems, Bournemouth, UK, 1977, p. 281.
[149] D.W. Shannon, in: Proceedings of USAEC Symposium on Zirconium Alloy Development, Vol. II, Castlewood, CA, USA, GE Report GEAP-4089, November 1962, Paper 18.
[150] R.C. Asher, B. Cox, in: Proceedings of IAEA Conference on Corrosion of Reactor Materials, Salzburg, AU, STI Pub59, Vol. 2, June 1962, p. 209.
[151] T. Isobe, T. Murai, Y. Mae, in: E.R. Bradley, G.P. Sabol (Eds.), Proceedings of 11th International Symposium on Zr in the Nuclear Industry, Garmisch-Partenkirchen, Germany, ASTM-STP-1295, American Soc. for Testing and Mater., W. Conshohocken, PA, USA, 1996, p. 203.
[152] H.G. Weidinger, H. Ruhmann, G. Cheliotis, M. Maguire, T.-L. Yau, in: C.M. Eucken, A.M. Garde (Eds.), Proceedings of 9th International Symposium on Zr in the Nuclear Industry, Kobe, Japan, ASTM-STP-1132, American Soc. for Testing and Mater., Philadelphia, PA, USA, 1991, p. 499.
[153] P. Rudling, B. Lehtinen, Mechanistic Understanding of Nodular Corrosion, US Report, EPRI-TR-103396, Electric Power, Res. Inst., Palo Alto, CA, November 1993.
[154] M.O. Marlowe, J.S. Armijo, B. Cheng, R.B. Adamson, in: Proceedings of ANS Topical Meeting on LWR Fuel Performance, Vol. 1, Orlando, FL, American Nuclear Soc., La Grange Pk., ILL, USA, 1985, p. 373.
[155] F. Garzarolli, H.-J. Sell, J. Thomazet, PWR Li coolant chemistry and Fuel Cladding Performance, Presented at Jahrestagung Kerntechnik, 2002, INFORM, Bonn.
[156] P. Bossis, G. Lelievre, P. Barberis, X. Iltis, F. Lefebvre, in: G.P. Sabol, G.D. Moan (Eds.), Proceedings of 12th International Symposium on Zr in the Nuclear Industry, Toronto, Canada, ASTM-STP-1354, American Soc. For Testing and Mater., W. Conshohocken, PA, USA, 2000, p. 918.